geologicaacta

Citation: Santamaría-Pérez, E., Medina-Cascales, I., Martin-Rojas, I., Alfaro, P., 2026. Active faulting in the Betic External Zones (SE, Spain): The Alcoy Fault Zone. Geologica Acta, 24.4, 1-pgs. DOI: 10.1344/GeologicaActa2026.24.4
Online ISSN: 1696-5728

Active faulting in the Betic External Zones (SE, Spain): The Alcoy Fault Zone

Eva Santamaría-Pérez Iván Medina-Cascales Iván Martin-Rojas Pedro Alfaro

[1]Departamento de Ciencias de la Tierra y del Medio Ambiente, Universidad de Alicante
03690, San Vicente del Raspeig, Alicante, Spain. Santamaría-Pérez E-mail: eva.santamaria@ua.es;
Medina-Cascales E-mail: ivan.medina@ua.es; Martin-Rojas E-mail: ivan.martin@ua.es; Alfaro E-mail: pedro.alfaro@ua.es

ABSTRACT

Evidence of active faulting is presented from a fault in the eastern Betic External Zones (SE Spain). New fault data are provided for the Alcoy Fault Zone, a structure whose Quaternary activity is currently under debate. This study includes a detailed structural and geomorphic characterization, along with a preliminary palaeoseismological analysis. This fault is ca. 13km long, and two main sectors are defined based on its surface geometry: a SW sector striking N060E formed by a border fault strand, and a NE sector striking N040E to N065E, formed by a border and an intrabasinal fault strands. The Alcoy Fault Zone displays oblique kinematics, with a predominant left-lateral and a subordinate dip-slip component. Quaternary fault activity is evidenced by a qualitative and quantitative geomorphic analysis, where three geomorphic indices were applied (Smf, Vf, and Bs). The fault presents a marked mountain front with low sinuosity. Cross-fault streams, which are deflected in a left-lateral sense, exhibit knickpoints that coincide with the fault traces and display highly incised valleys. Moreover, the morphology of their watersheds is consistent with an ongoing tectonic uplift in the area. Additionally, the palaeoseismological analysis performed in deformed colluvial deposits suggests a Holocene surface rupture history involving two events during the last ca. 1160 years. The results of this work represent the first step for the seismogenic characterization of the Alcoy Fault Zone and the base for further seismic hazard assessment studies in the External Zones of the eastern Betic Cordillera. However, additional seismicity studies will be required to determine whether the fault is basement-involved or represents a decoupled structure controlled by the Triassic evaporitic layer between the Variscan basement and the pre-Neogene Betic rocks.

KEYWORDS **Fault characterization. Active tectonics. Tectonic geomorphology. Palaeoseismology. Betic External Zones.**

INTRODUCTION

In the Betic Cordillera (S Iberian Peninsula) (Fig. 1), the crustal deformation produced by the convergence between the Nubian and Eurasian plates is currently being accommodated by a wide number of active structures. This tectonic activity is responsible for a moderate seismic activity defined by frequent low-magnitude earthquakes and occasional moderate to strong events with magnitudes higher than 5 (Fig. 1; Buforn *et al.*, 2004; Delgado *et al.*, 1993; Muñoz and Udías, 1981; 1991; Rueda *et al.*, 1996; and references therein). Deformation is accommodated differently in the two main domains of the Betic Cordillera –the Betic Internal Zones and the Betic External Zones–, resulting in marked differences in the seismicity.

Most of the characterized active faults in the Betic Cordillera are concentrated in the Betic Internal Zones, where the seismic activity is more intense (Fig. 1). The most significant active faults defined in the Quaternary Active Faults Database of Iberia (QAFI, García-Mayordomo *et al.*, 2012) are found within the so-called Eastern Betic

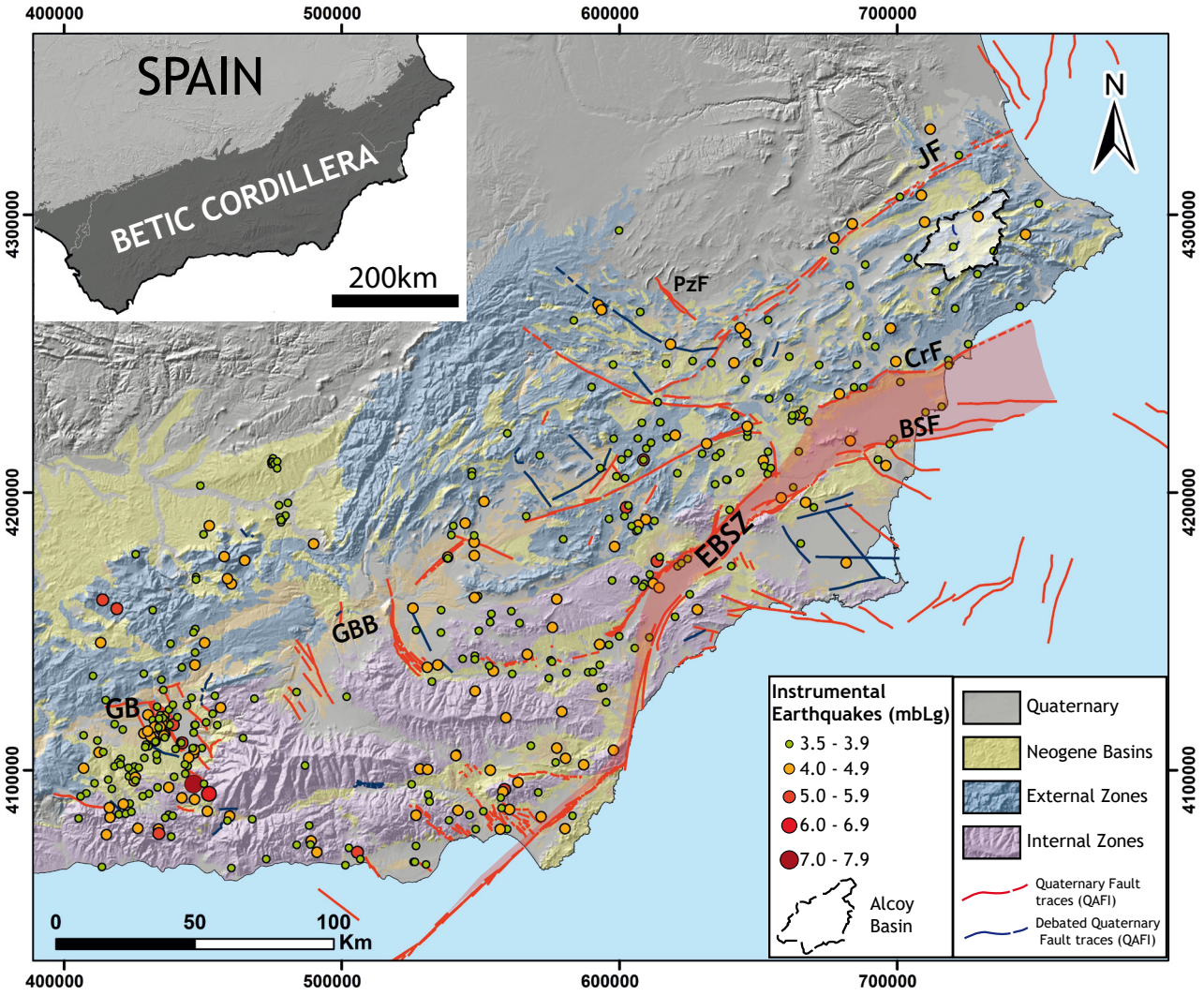

FIGURE 1. Geological map of the eastern Betic Cordillera with the Alcoy Basin location and the instrumental seismic records with magnitudes greater than 3.5. GB: Granada Basin; GBB: Guadix-Baza Basin; BSF: Bajo Segura Fault; CrF: Crevillente Fault; PzF: Pozohondo Fault; JF: Jumilla Fault.

Shear Zone (EBSZ, *e.g.* Bousquet, 1979; De Larouzière *et al.*, 1988; Montenat *et al.*, 1987; Silva *et al.*, 1993), the Granada Basin (*e.g.* Madarieta-Txurruka *et al.*, 2021; Ruano *et al.*, 2004; Sanz de Galdeano *et al.*, 2012), the Guadix-Baza Basin (*e.g.* Alfaro *et al.*, 2008; Medina-Cascales *et al.*, 2021), and the province of Almería (Galindo-Zaldívar *et al.*, 2013; Marín-Lechado *et al.*, 2005, 2010; Sanz de Galdeano *et al.*, 2010). These structures accommodate a large portion of crustal shortening and are responsible for significant seismic activity. Therefore, most of the active tectonics studies in the Betic Cordillera are focused on these faults.

In contrast, in the Betic External Zones, the number of active faults defined in the QAFI database is significantly lower (García-Mayordomo *et al.*, 2012). As this domain is located farther from the plate boundary, the seismic activity is less intense. Therefore, the number of detailed studies focused on active tectonics is considerably lower than in the Betic Internal Zones.

This is the case for the eastern sector of the Betic Cordillera, where the study area of this work is located. In this sector, most of the studied faults are those within the Internal Zones—particularly the ones in the EBSZ (Alfaro, 1995; Alfaro *et al.*, 2002, 2012; Batlló *et al.*, 2015; Borque *et al.*, 2019; García-Mayordomo 2005; Martin-Rojas *et al.*, 2014, 2015; Perea *et al.*, 2012; Sánchez-Alzola *et al.*, 2014; Soria *et al.*, 2001; Taboada *et al.*, 1993). On the other hand, in the Betic External Zones, north of the EBSZ, only a few faults have been reported as currently active, while the Quaternary activity of other structures remains a subject of debate (Fig. 1) (Canora, 2005; García-Mayordomo, 2005; Rodríguez-Pascua *et al.*, 2008, 2012; Zazo *et al.*, 1993).

However, although the knowledge about the active faults in the easternmost sector of the External Zones is limited, there are significant earthquakes documented in the historical seismic records (Martínez-Solares and Mezcua, 2002). These events had strong destructive effects, resulting in numerous casualties and severe structural damages. The most relevant earthquakes include the Tavernes de la Valldigna event (1395–1396; Instensity European Macroseismic Scale, IEMS-98= VIII–IX; Giner *et al.*, 2003; López-Marinas, 1981), the Alcoy earthquake (1620; IEMS-98= VIII–IX), the seismic sequence of Muro (1644; IEMS-98= VII–VIII) (Buforn and Udías, 2021, 2022; Martínez-Solares and Mezcua, 2002), and the two Estubeny earthquakes (1748; IEMS-98= IX and IEMS-98= VII–VIII, respectively; Bisbal-Cervelló, 1984; Martínez-Solares and Mezcua, 2002).

Two of these destructive events, the 1620 Alcoy earthquake and the 1644 Muro seismic sequence, took place in the study area, located in the Alcoy Basin. Based on pre-instrumental seismic events, early seismic hazard assessments classified this area as having a high potential for destructive earthquakes (López-Casado *et al.*, 1987). Moreover, the urban areas of the Alcoy Basin are especially vulnerable to seismically induced landslides due to the abundance of very steep river valleys and weak marly soils (Delgado *et al.*, 2006; Martino *et al.*, 2018; Tomás *et al.*, 2023). However, despite the inferred seismic hazard and the historical and instrumental seismicity, the information available about the seismogenic sources responsible for the 1620 and 1644 events is very limited due to the scarce studies on active tectonics in the Alcoy Basin. Previous studies in the basin were focused on its Neogene tectono-sedimentary evolution (*e.g.* De Ruig, 1992; Ott d'Estevou *et al.*, 1988; Pierson d'Autrey, 1987), the compilation and analysis of historical seismic records and their macroseismic effects (Buforn and Udías, 2021, 2022), and proposed seismic zonations based on seismic and geological data (García-Mayordomo, 1998, 2005).

Three potentially active faults have been previously defined in the Alcoy Basin: the Alcoy-Cocentaina Fault, the Mariola Fault, and the Benasau Fault (Fig. 2; García-Mayordomo, 1998, 2005; García-Mayordomo *et al.*, 2002). However, the Quaternary activity of these structures remains a subject of debate (*e.g.* García-Mayordomo, 1998; Pierson d'Autrey, 1987; Zazo *et al.*, 1993). The lack of detailed structural and active tectonic analyses prevents a more precise assessment of their possible recent activity and seismogenic potential.

The present study is focused on the Alcoy-Cocentaina Fault, in this work renamed as the Alcoy Fault Zone (AFZ). The AFZ was defined as a SW-NE strike-slip fault, being one of the main structures in the Alcoy Basin (García-Mayordomo, 1998; Pierson d'Autrey, 1987; Zazo *et al.*, 1993). It is a critical structure, since it partially crosses the city of Alcoy. However, the Quaternary activity of the AFZ is under consideration, since it has been described both as an inactive structure since the Messinian (Pierson d'Autrey, 1987) or as an active fault based mainly on geomorphic evidence (García-Mayordomo, 1998; Zazo *et al.*, 1993). Moreover, it was proposed as a potential seismogenic source of the 1620 Alcoy earthquake (García-Mayordomo, 1998; Zazo *et al.*, 1993). Nevertheless, the absence of absolute dating of the tectonic geomorphic features related to the fault made impossible to provide robust evidence about the current activity of the AFZ.

The main aim of this study is to present a new detailed characterization of the AFZ and provide new evidence of the Quaternary activity of this structure. For this purpose, structural, geomorphological, and palaeoseismological analyses were carried out. New data are presented, including a detailed geological and structural map. New evidence of Quaternary activity is provided through two different approaches. First, the geomorphological impact of the fault activity on the quaternary landscape is analysed qualitatively and quantitatively through the application of several geomorphic indices. Second, new outcrops showing deformed Quaternary deposits are presented, including absolute radiocarbon dating and a palaeoseismological analysis. The ultimate objective of this work is to improve the amount of information available about the AFZ in a region with relevant historical seismicity.

GEODYNAMIC AND SEISMOLOGICAL SETTING

Since the Late Miocene, the western Mediterranean region has been characterized by the convergence of the Nubian and Eurasian plates. This convergence is approximately 5–6 mm/year in a NW-SE motion (Argus *et al.*, 2011; DeMets *et al.*, 2010; Nocquet, 2012; Pérez-Peña *et al.*, 2010; Serpelloni *et al.*, 2007). About one-third of this convergence is accommodated in SE Iberia and the Algero-Balearic Basin (Borque *et al.*, 2019; Echeverria *et al.*, 2013, 2015; Serpelloni *et al.*, 2007).

In the eastern sector of the Betic Cordillera, the plate convergence is responsible for NNW-SSE shortening, which is mainly accommodated by the faults forming the EBSZ (Bousquet, 1979; De Larouzière *et al.*, 1988; Silva *et al.*, 1993) —such as the Bajo Segura Fault (Alfaro, 1995; Alfaro *et al.*, 2002, 2012; Borque *et al.*, 2019; García-Mayordomo, 2005; Perea *et al.*, 2012; Sánchez-Alzola *et al.*, 2014; Taboada *et al.*, 1993) and the Crevillente Fault (Martin-Rojas *et al.*, 2014, 2015; Soria *et al.*, 2001).

On the other hand, the characteristics of the deformation partitioning north of the EBSZ, in the Betic External Zones,

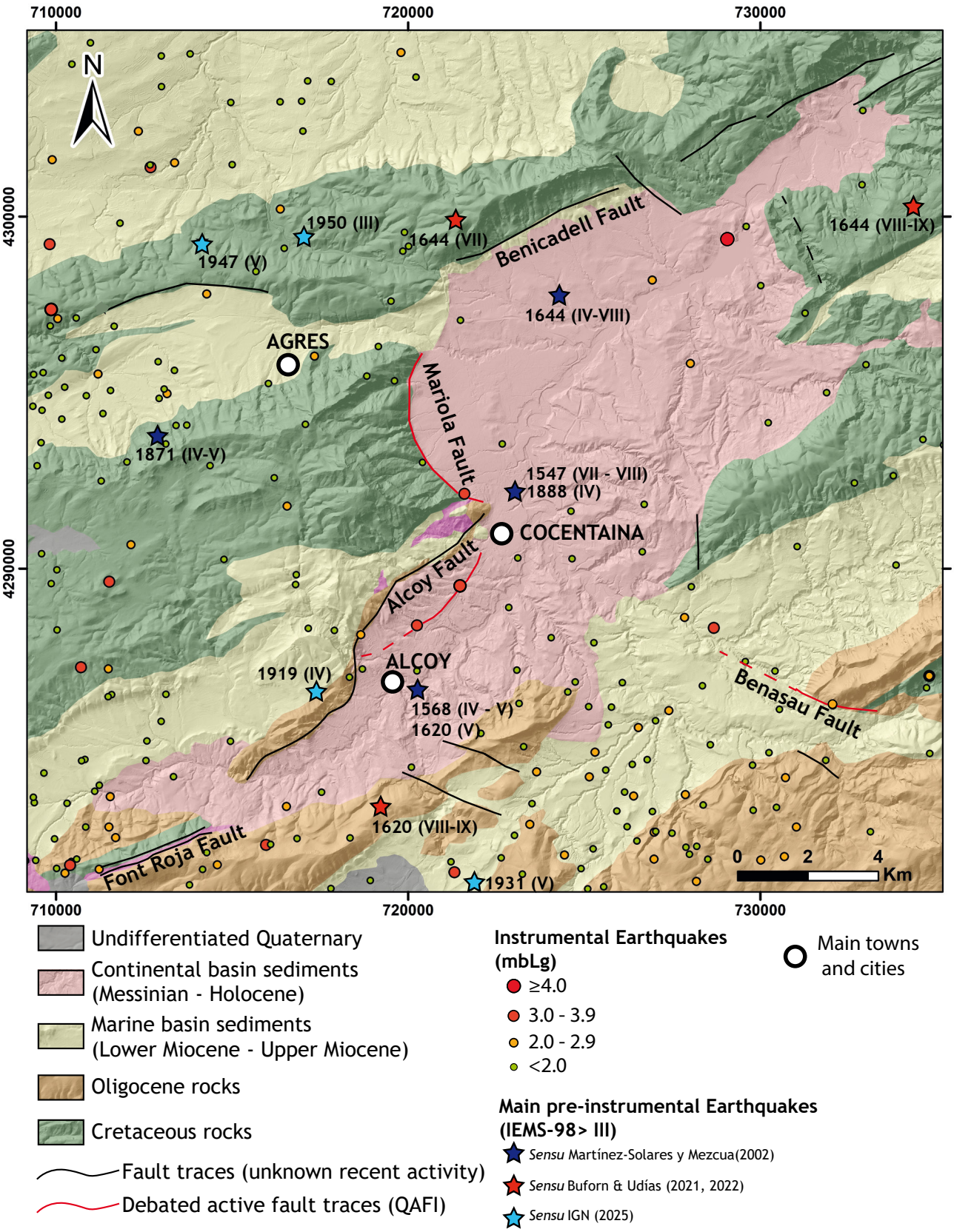

FIGURE 2. Seismotectonic map of the Alcoy Basin (Instrumental Earthquakes source: IGN, 2025).

remain largely unknown. There are only a few defined faults that may be accommodating part of the deformation during the Quaternary. These are the Jumilla Fault (García-Mayordomo, 2005; Goy *et al.*, 1987; Van Balen *et al.*, 2015), the western section of the Crevillente Fault (Canora, 2005), and the Pozohondo Fault (Rodríguez-Pascua *et al.*, 2008, 2012). Moreover, other faults, whose Quaternary activity is under discussion, have been identified in the Alcoy Basin (García-Mayordomo, 1998, 2005; García-Mayordomo *et al.*, 2002). The Alcoy Basin is a Neogene-Quaternary intramontane basin in the eastern Betic Cordillera (Fig. 1) that formed as a result of extensional tectonics during late Miocene times (De Ruig, 1992). The Neogene-Quaternary materials of the Alcoy Basin are deposited over Mesozoic to Paleogene rocks belonging to the Prebetic domain of the Betic External Zones (Fig. 2) (Azéma *et al.*, 1979; De Ruig, 1992; Fallot, 1948; García-Hernández *et al.*, 1980; Pierson d'Autrey, 1987 and references therein). These pre-Neogene rocks are separated from the Variscan basement by a layer of Triassic evaporites, which constitutes a mechanical weak layer from a rheological point of view. This evaporitic layer played a relevant role during the Miocene, leading to the formation of different diapiric structures (Canova *et al.*, 2025; De Ruig, 1992; Martínez del Olmo *et al.*, 1986; Moseley *et al.*, 1981; Pedrera *et al.*, 2014; Roca *et al.*, 2006; Rubinat *et al.*, 2010, 2012).

The sedimentary infill of the Alcoy Basin consists mainly of Langhian to Early Messinian marine deposits overlain by Messinian-Pliocene continental sediments (De Ruig, 1992; Mansino *et al.*, 2013; Ott d'Estevou *et al.*, 1988; Pierson d'Autrey, 1987). These continental deposits consist of alluvial conglomeratic materials in the basin margins and a thick lacustrine succession towards the basin depocenter. The Quaternary sedimentation consists of large Middle to Upper Pleistocene alluvial fan systems (Molina-Hernández *et al.*, 2015, 2016; Van Der Made and Montoya, 2007), slope deposits, and several sequences of fluvial terraces and travertinic platforms (Bernabé-Maestre, 1975; Estrella *et al.*, 1993; Fumanal, 1994; Ordóñez-Delgado *et al.*, 2016; Pierson d'Autrey, 1987).

The basin boundaries are defined by a series of Neogene anticlines and faults (De Ruig, 1992). These border faults are the Alcoy Fault Zone, the Mariola Fault, the Benicadell Fault, the Benasau Fault, and the Font Roja Fault (Fig. 2). All these faults affect the infill deposits of the Alcoy Basin. Among these structures, the Alcoy Fault Zone, the Mariola Fault, and the Benasau Fault have been proposed as potential seismogenic sources (Fig. 2; García-Mayordomo, 1998, 2005; García-Mayordomo *et al.*, 2002).

The Alcoy Basin presents historical seismic records and an ongoing seismic activity. The most significant pre-instrumental historical seismic events in the Alcoy Basin are the 1620 Alcoy Earthquake and the 1644 Muro seismic series (Buforn and Udías, 2021, 2022, and references therein). The 1620 Alcoy earthquake occurred on December the 2nd, followed by 33 aftershocks. Another significant event struck on December the 14th (Carbonell, 1668), with seismic activity continuing until January the 14th, 1621. The main shock caused extensive damage in Alcoy city (over 60% of houses destroyed, partial or total collapse of city walls, churches, monasteries, and towers) and affected nearby towns. Casualty estimates exceed 200 deaths (García-Molero, 1621). Ground effects included large fissures and earthquake-induced landslides that caused parts of the town to collapse into river gorges (Delgado *et al.*, 2006). The maximum intensity (IEMS-98) calculated for the main event vary between VII–VIII (Martínez-Solares and Mezcúa, 2002), and VIII–IX (Buforn and Udías, 2021, 2022). Estimated magnitude ranges between 4.9 mb/4.6 MS (Delgado *et al.*, 2006) and 5.5 Mw (Delgado *et al.*, 2011). The 1644 Muro de Alcoy seismic series took place throughout June 1644, with three main events on the 15th, 19th, and 26th of June. It affected a broader area than the 1620 earthquake, with damage extending to coastal towns 30 km away. The most destructive event was on June 26th, felt even in Valencia (over 70 km away). Casualties count is very difficult to assess, but minimun of 20 fatalities is estimated, and some historical records speak about small and isolated towns being completely destroyed. Estimated maximum intensities (IEMS-98) are IV–V (Martínez-Solares and Mezcúa, 2002) and VII (Buforn and Udías, 2021, 2022) for the events of the 15th and the 19th of June, respectively. For the 26 June event, the proposed intensities range between VIII (Martínez-Solares and Mezcua, 2002) and VII–IX (Buforn and Udías, 2021, 2022). The proposed seismogenic source or the 1644 Muro de Alcoy seismic series is an ENE–WSW oriented fault system at the northern border of the Alcoy basin (Buforn and Udías, 2022), but no detailed information on the specific structures or their characteristics is available for neither the 1620 Alcoy Earthquake or the 1644 Muro de Alcoy series. Other than these two events, a total of 36 significant pre-instrumental earthquakes (dating from 1258 to 1893) have been documented in the basin (Martínez-Solares and Mezcua, 2002; Buforn and Udías, 2021, 2022; Table 1). The most significant ones are the 1258 Ontinyent (IEMS-98= VIII sensu Martínez-Solares and Mezcua, 2002) and the 1547 Cocentaina (IEMS-98= VII–VIII sensu Martínez-Solares and Mezcua, 2002) earthquakes, but the precise locations of their epicenters are unknown.

During the instrumental period in this region, which extends from the late 1950s to the present, more than 300 earthquakes have been recorded within the Alcoy Basin and nearby areas. These events predominantly display low magnitudes, although several have exceeded magnitude 3 mbLg, with a maximum recorded magnitude of 4.8 mbLg (Fig. 2; IGN, 2025). Some of these earthquakes were

TABLE 1. Main pre-instrumental earthquakesin the Alcoy Basin and surroundings

Location	Date	Lat	Long	I (EMS-98)	Reference	Comments
Ontinyent	March 1258	0º 36' W	38º 50'	VIII	Martínez-Solares and Mezcua (2002)	
Cocentaina	29 Agost 1547	0º 26' W	38º 45'	VII-VIII	Martínez-Solares and Mezcua (2002)	
Alcoy	29 January 1568	0º 28' W	38º 42'	IV-V	Martínez-Solares and Mezcua (2002)	
Ontinyent	7 October 1615	0º 34' W	38º 48'	*unknown*	Martínez-Solares and Mezcua (2002)	
Alcoy	2 December 1620	0º 28' 48" W	38º 40'	VIII-IX	Bufforn and Udías (2021, 2022)	Main event
Alcoy	14 December 1620	0º 28' W	38º 42'	V	Martínez-Solares and Mezcua (2002)	Aftershock
Alcoy	18 December 1620	0º 28' W	38º 42'	*unknown*	Martínez-Solares and Mezcua (2002)	Aftershock
Alcoy	25 December 1620	0º 28' W	38º 42'	*unknown*	Martínez-Solares and Mezcua (2002)	Aftershock
Alcoy	6 January 1621	0º 28' W	38º 42'	*unknown*	Martínez-Solares and Mezcua (2002)	Aftershock
Alcoy	14 January 1621	0º 28' W	38º 42'	*unknown*	Martínez-Solares and Mezcua (2002)	Aftershock
Alcoy	21 January 1621	0º 28' W	38º 42'	*unknown*	Martínez-Solares and Mezcua (2002)	Aftershock
Muro de Alcoy	14 June 1644	0º 25' W	38º 48'	IV-V	Martínez-Solares and Mezcua (2002)	Premonitory
Muro de Alcoy	15 June 1644	0º 13' 12" W	38º 51' 00"	VII	Bufforn and Udías (2021, 2022)	First main
Muro de Alcoy	19 June 1644	0º 27' W	38º 49' 12"	VII	Bufforn and Udías (2021, 2022)	Second main
Muro de Alcoy	26 June 1644	0º 18' 0"W	38º 49' 12"	VIII-IX	Bufforn and Udías (2021, 2022)	Third main
Alcoy	1727	0º 28' W	38º 42'	*unknown*	Martínez-Solares and Mezcua (2002)	
Alcoy	1752	0º 28' W	38º 42'	*unknown*	Martínez-Solares and Mezcua (2002)	
Alcoy	2 November 1753	0º 28' W	38º 42'	*unknown*	Martínez-Solares and Mezcua (2002)	
Alcoy	19 November 1753	0º 28' W	38º 42'	*unknown*	Martínez-Solares and Mezcua (2002)	
Ontinyent	1 November 1755	0º 36' W	38º 49'	IV-V	Martínez-Solares and Mezcua (2002)	
Alcoy	5 May 1756	0º 28' W	38º 42'	*unknown*	Martínez-Solares and Mezcua (2002)	
Alcoy	26 September 1793	0º 28' W	38º 42'	V	Martínez-Solares and Mezcua (2002)	
Alcoy	2 November 1819	0º 28' W	38º 42'	IV	Martínez-Solares and Mezcua (2002)	
Alcoy	2 November 1819	0º 28' W	38º 42'	V	Martínez-Solares and Mezcua (2002)	
Alcoy	2 November 1819	0º 28' W	38º 42'	IV	Martínez-Solares and Mezcua (2002)	
Cocentaina	27 December 1858	0º 26' W	38º 45'	*unknown*	Martínez-Solares and Mezcua (2002)	
Alcoy	30 December 1869	0º 28' W	38º 42'	III-IV	Martínez-Solares and Mezcua (2002)	
Alcoy	5 May 1871	0º 28' W	38º 42'	III	Martínez-Solares and Mezcua (2002)	
Alfafara	19 November 1871	0º 33' W	38º 46'	IV-V	Martínez-Solares and Mezcua (2002)	
Alcoy	29 July 1872	0º 28' W	38º 42'	III-IV	Martínez-Solares and Mezcua (2002)	Main event
Alcoy	30 July 1872	0º 28' W	38º 42'	III	Martínez-Solares and Mezcua (2002)	Aftershock
Alcoy	8 November 1882	0º 28' W	38º 42'	V	Martínez-Solares and Mezcua (2002)	Main event
Alcoy	12 November 1882	0º 28' W	38º 42'	III-IV	Martínez-Solares and Mezcua (2002)	Aftershock
Cocentaina	18 December 1888	0º 26' W	38º 45'	IV	Martínez-Solares and Mezcua (2002)	
Alcoy	13 October 1890	0º 28' W	38º 42'	IV	Martínez-Solares and Mezcua (2002)	
Alcoy	2 September 1893	0º 28' W	38º 42'	IV-V	Martínez-Solares and Mezcua (2002)	
Alcoy	20 January 1919	-0.5	38.7	IV	IGN (2025)	
Alcoy	28 January 1931	-0.45	38.65	V	IGN (2025)	
Agullent	27 July 1947	-0.5333	38.8167	V	IGN (2025)	
Vall de Gallinera	28 January 1950	-0.5	38.8167	III	IGN (2025)	

felt across several towns, so their estimated maximum intensities range from II to IV (IEMS-98; IGN, 2025).

METHODOLOGY

The surface trace of the AFZ was defined through detailed field geological and structural mapping of the study area. Apart from field observations, recent and historical aerial photography, as well as high-resolution digital elevation models (DEM of 2 m per pixel resolution) were analysed. In addition to the geometry of the fault traces, the resulting geological map includes a new detailed surveying of the previously defined lithostratigraphic units that crop out in the area (Fig. 3).

From a geomorphological point of view, recent fault activity was assessed by means of a qualitative and quantitative geomorphic analysis. High-resolution Digital Elevation Models (DEMs) were used as the basis for these spatial analyses. The qualitative geomorphic assessment consisted of an analysis of anomalies in the geometry of the drainage network (*i.e.* offset, displaced, beheaded or captured fluvial valleys and river streams). This was complemented with an analysis of the channel morphology of 12 topographic stream profiles crossing the fault zone.

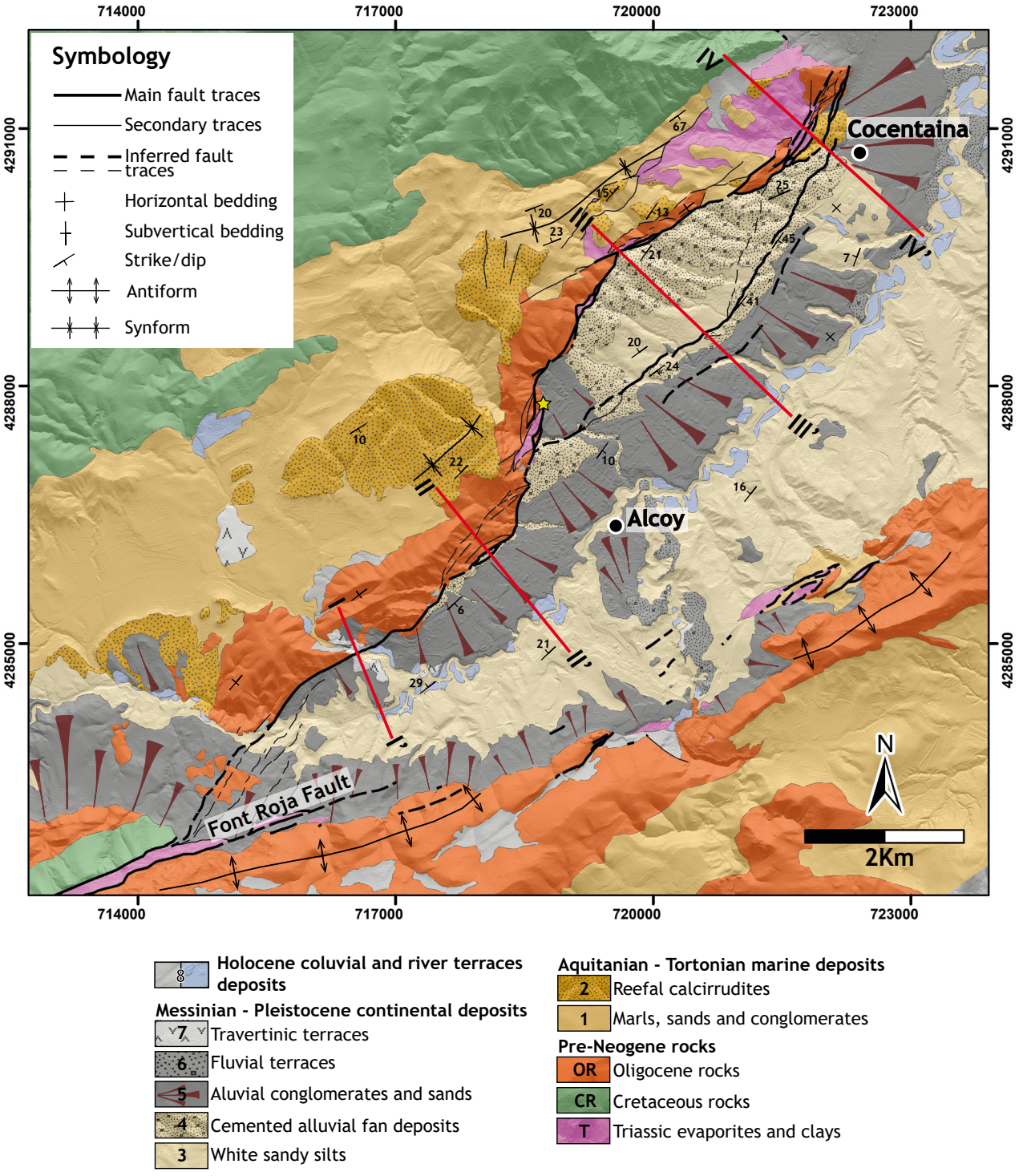

FIGURE 3. Geological map of the study area, including the new detailed trace of the Alcoy Fault Zone. Red lines mark de position of the geological sections in Figure 5. The yellow star shows the location of the Cotes Altes) site, where the palaeoseismological analysis was performed.

These profiles provide useful insights about the relationship between tectonics and erosion (*e.g.* Bull, 2009; Keller and Pinter, 2002; Schumm *et al.*, 2000). Concave shapes suggest equilibrium conditions, while sub-linear to convex profiles could be indicative of tectonic influence, aside from lithological contrasts and environmental or basement level changes (Hack, 1973; Snyder *et al.*, 2000; Soria-Jáuregui *et al.*, 2018). The quantitative geomorphic assessment consisted of the application of three geomorphic indices that were calculated: the mountain front Sinuosity index (Smf) (Bull and McFadden, 1977; Wells *et al.*, 1988), the Valley width/height ratio (Vf) (Bull and McFadden, 1977), and drainage Basin shape index (Bs) (Canon, 1976; Ramírez-Herrera, 1994).

The mountain front Smf (Bull and McFadden, 1977; Wells *et al.*, 1988) was calculated. This index compares the difference between sinuous and straight mountain fronts using the total length value versus the length of a straight line parallel to the studied front. This index is defined as:

$$Smf = Lmf/Ls \quad (1)$$

Where Lmf is the total length of the mountain front, and Ls is the length along a straight line parallel to the front.

Vf (Bull and McFadden, 1977) reflects the difference between valleys with active down-cutting response to base-level unstability (V-shaped valleys with Vf values lower than 1.0), and valleys with a predominant lateral erosion due to relative stable base-level response (U-shaped valleys with Vf values higher than 1.0) (Silva *et al.*, 2003). It is defined as follows:

$$Vf = 2Vfw/((Eld-Esc)+(Erd-Esc)) \quad (2)$$

Where Vfw is the width of the valley floor, Eld and Erd are the elevations of both sides of the valley (left and right, respectively), and Esc is the elevation of the valley floor or stream channel. Transverse profiles were traced across the 12 selected streams and gorges at 250m upstream from the mapped mountain front, as indicated by Silva *et al.* (2003). From all these profiles, the valley floor width, the elevations of the right and left sides of the watershed, and the height of the valley floor were extracted for the calculation of the Vf index.

Finally, the planimetric shape of a basin may be numerically described by the drainage Bs or longitude versus width (l/w) ratio (Canon, 1976; Ramírez-Herrera, 1994). The index reflects the degree of elongation of a basin, and is expressed as:

$$Bs = Bl/Bw \quad (3)$$

Where Bl is the length of the basin from its mouth to the most distant divide, and Bw is the width measured across the short axis perpendicular to Bl measure.

Finally, the Quaternary activity of the AFZ was also assessed using a palaeoseismological approach. An outcrop exhibiting deformed Quaternary deposits was selected for a preliminary palaeoseismological survey (see location in Fig. 3). This outcrop was selected due to the presence of datable levels. Seven radiocarbon samples were collected, including 3 bulk samples and 4 gastropod shells. Then, the numerical data were integrated in a Bayesian statistics analysis using the OxCal software (Bronk Ramsey, 2008, 2009), obtaining Probability Density Functions (PDFs) that provided a date for the identified events.

CHARACTERIZATION OF THE ALCOY FAULT ZONE

Fault zone surface geometry and structure

The AFZ is a ca. 13km long fault zone striking SW-NE with a predominant direction of N045E (Fig. 3). The fault zone is formed by fault planes that dip vertically, or steeply to the SE (Fig. 4), and locally some smaller planes that dip to the NW. Based on the fault surface geometry, the AFZ can be divided into two sectors separated by a marked fault bend: the SW sector and the NE sector (Fig. 5).

The SW sector runs 5.5 km from the southern termination of the fault to the city of Alcoy (Figs. 3; 5). In this sector, the AFZ strikes roughly N060E, with planes ranging from N030E to N065E and dipping sub-vertically or steeply to the SE (sections I-I' and II-II' in Fig. 4). These planes typically exhibit slickenlines with rakes between 10ºNE and 25ºNE. Smaller fault planes striking N-S are also present at some localities, with slickenline rakes varying from 60ºE to 85ºE. Very locally, some planes display slickenlines with lower (0ºNE and 12ºNE) and higher (87ºSE and 90ºSE) rakes (Fig. 6C, D). Nevertheless, most of the measured slickenlines in the SW sector indicate a predominant oblique motion with a main strike-slip component and a secondary dip-slip component.

In this sector, the AFZ consists of a border fault that separates Oligocene carbonate conglomerates in the footwall from the Neogene lacustrine marls of the basin infill in the hanging-wall, forming a marked fault scarp (*e.g.* section I-I' in Fig. 4). These lacustrine marls are tilted ca. 20ºNW towards the fault (Fig. 3; 4). To the SW, the fault zone splits into several secondary, subparallel strands that offset the hanging-wall, forming an 800 m-wide damage zone with a "horsetail-like" geometry. Towards the SW, the AFZ terminates by linking with the N070E Font Roja

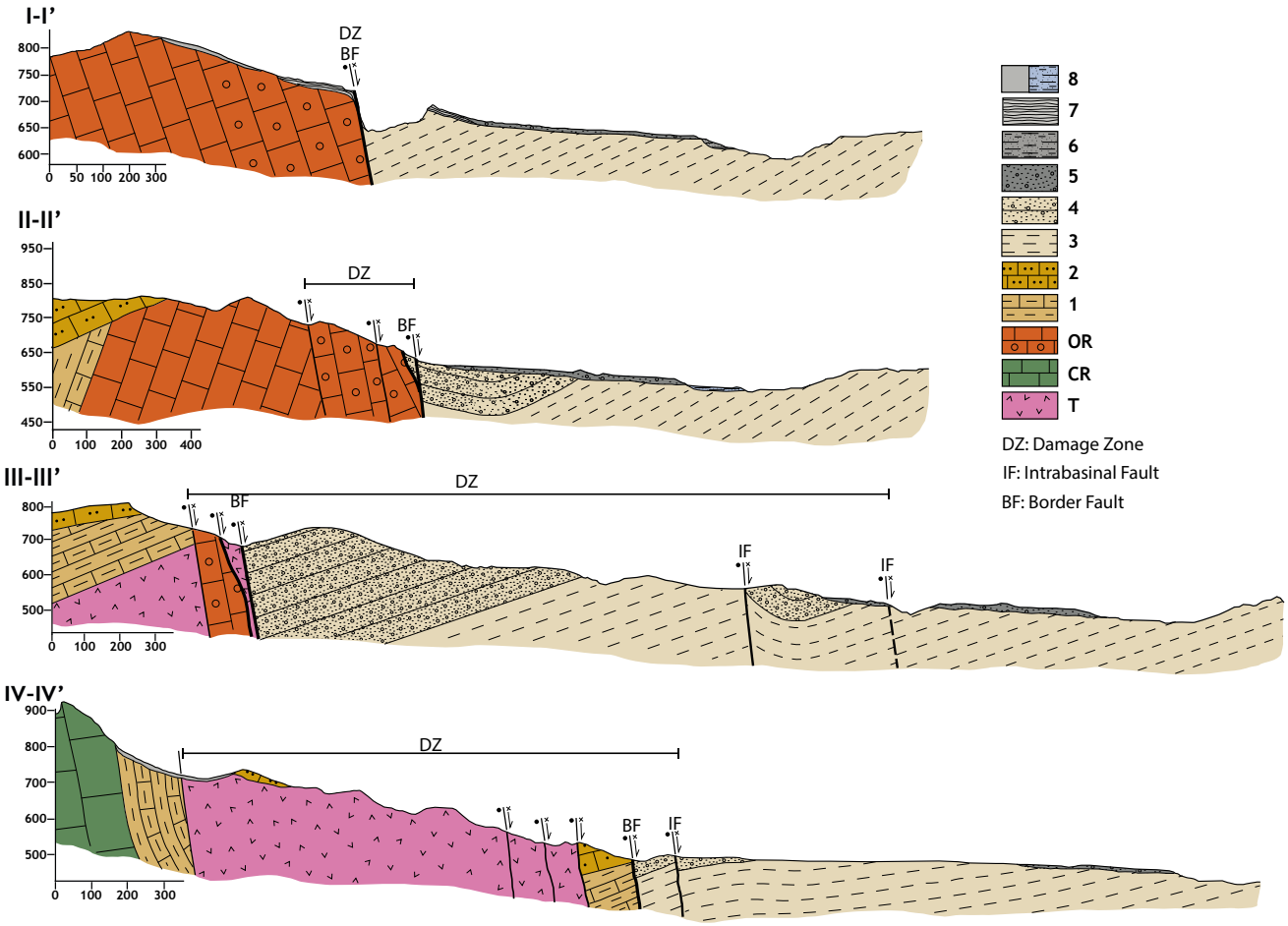

FIGURE 4. Geological cross-sections along the Alcoy Fault Zone. Locations are indicated in Figure 3. Units descriptions are shown in Figure 3.

Fault (Fig. 3; 5). To the NE, towards the city of Alcoy, the AFZ locally widens up to 300 m, comprising several intra-Oligocene secondary traces (Fig. 6A) displaying a complex geometry (Fig. 5).

The NE sector extends 7.5 km between the cities of Alcoy and Cocentaina (Figs. 3; 5). The surface geometry of this sector presents more complexity. Two main fault strands were identified in this sector: a border fault zone to the NW and an intrabasinal fault zone to the SE (Figs. 3; 5). Therefore, the width of the damage zone in this sector ranges from a few tens of meters to 2100 m (sections III-III' and IV-IV' in Fig. 4).

The border strand is comprised by sections with different strike, resulting in a curved trace. Thus, from the end of the SW sector, the fault turns N10E forming a marked fault bend. To the NE, the fault gradually turns N040E and N065E (Figs. 3; 5). The exposed fault surfaces dip from 50ºSE (Fig. 6B) to vertically, or even steeply to the NW. Slickenlines in the border fault are neither abundant nor well preserved in the NE sector, but those that were measured display rakes between 4ºNE and 12ºNE, indicating a strike-slip displacement. Close to the fault bend, some planes present slickenlines with rakes ranging between 77ºNE and 89ºNE, indicating a local predominant dip-slip motion.

This border fault separates the Oligocene to early Tortonian rocks in the northwestern block from the Messinian to early Pliocene lacustrine marls and Pliocene alluvial fan conglomerates in the southeastern block (Figs. 3; 4). The northwestern block is offset by secondary strands displaying straight, curved, and anastomosed patterns, resulting in several topographic steps in the landscape (Fig. 4). Notably, in the southeastern block, the Messinian and Pliocene deposits are tilted ca. 20º towards the fault, which could indicate to a listric geometry of the fault at a deeper structural level (Figs. 3; 4). A characteristic feature along this fault zone is the presence of fault-bounded diapiric bodies of Triassic clays and evaporites belonging to the Keuper facies (Figs. 3; 4).

The intrabasinal strand extends ca. 5km, striking N030E to N055E with a curved trace and dipping sub-vertically or

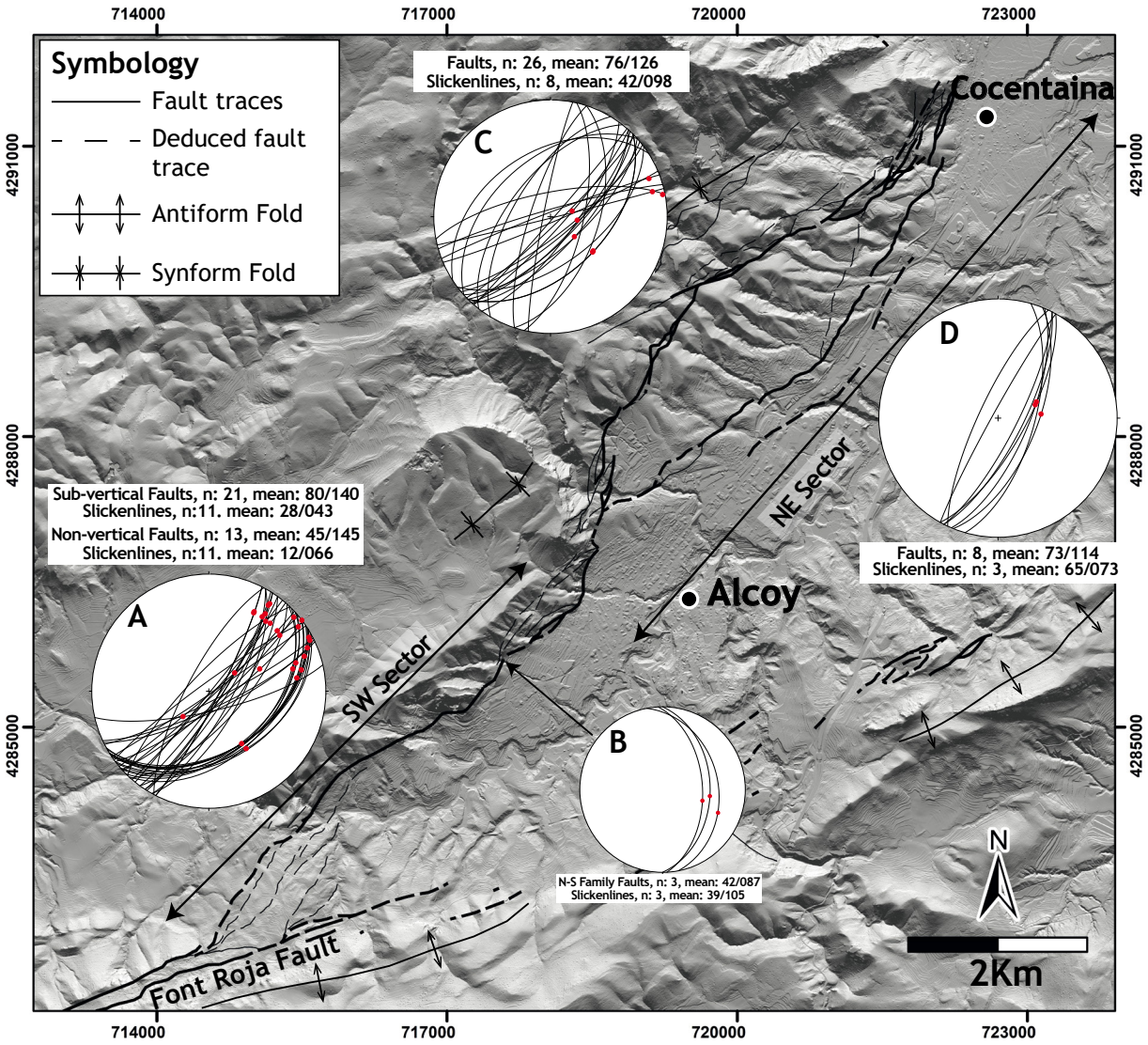

FIGURE 5. Map of the Alcoy Fault zone (AFZ) trace, showing the main structural features of the two sectors of the fault. Structural data, including fault plane and slickenline measures collected along the different fault strands, are plotted. A: SW sector; B: Minor N-S planes in the SW sector; C: NE sector, border fault; D: NE sector, intrabasinal fault.

locally steeply to the SE (Fig. 7A). Preserved slickenlines on its fault planes are very scarce, but are predominantly oblique with rakes ranging from 68ºNE to 77ºNE. This fault zone offsets the Messinian-Pliocene sediments from the Alcoy Basin infill. The fault trace is obscured and highly anthropized due to the intensly urbanized areas. There are few outcrops where the fault is exposed, some of them exhibiting meso-scale transpressive structures that deform the distal facies of the Pliocene alluvial fans and the lacustrine sediments (Fig. 7B). In the hanging-wall, a drag synform is developed in the alluvial and lacustrine materials, which dip varies between 40º and 50ºSE close to the fault zone (section III-III' in Figs. 4; 7C). From this fault zone towards the basin depocenter, the Messinian-Pliocene sediments display a consistent regional tilting of 20º towards the AFZ (Fig. 4). Close to the NE termination of the AFZ, the intrabasinal strand joins the border strand, forming a ca. 450m-wide band comprised by several sub-parallel strands and some secondary anastomosing short faults (Fig. 5). A remarkable feature in this termination is that is the only spot along the AFZ where Tortonian shallow marine deposits can be found in the southeast block of the border fault zone (Fig. 3 and section IV-IV' in Fig. 4).

The mapped pattern of the fault traces combined with the slickenline measures strongly suggest that the NNE-trending central part of the AFZ (southern part of NE sector in Figs. 3; 5) constitutes a releasing bend with predominant normal slip, between the NE-SW trending strike-slip segments of the SW sector and northern NE sector. Increased subsidence

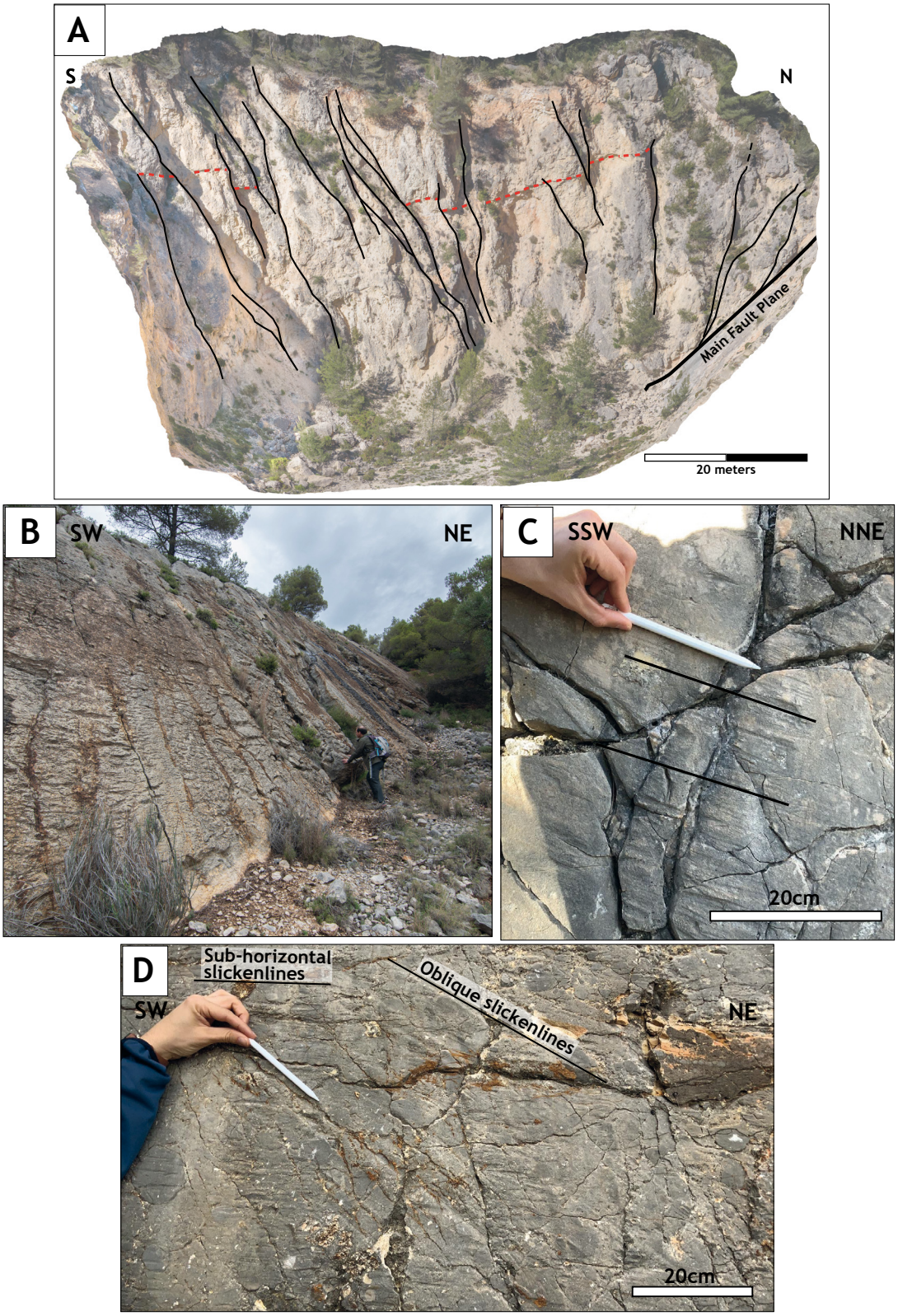

FIGURE 6. A) Example of a complex fault zone in the SW sector offsetting Oligocene conglomerates and limestones. Local sub-horizontal stratigraphy of the Oligocene rocks is marked by the dashed orange lines. Picture location: 30S 717390 m E 4285670 m N. B) Example of local normal faults. Picture location: 30S 718770 m E 4288283 m N. C) Oblique slickenlines on a preserved fault plane of the SW sector of the AFZ. Pircture location: 30S 715552 m E 4284227 m N. D) Different families of slickenlines are observable in the same fault plane: sub-horizontal, and oblique slickenlines. Picture location: 30S 717380 m E 4285680 m N. Projected coordinate system: ETRS 1989, UTM Zone 30N.

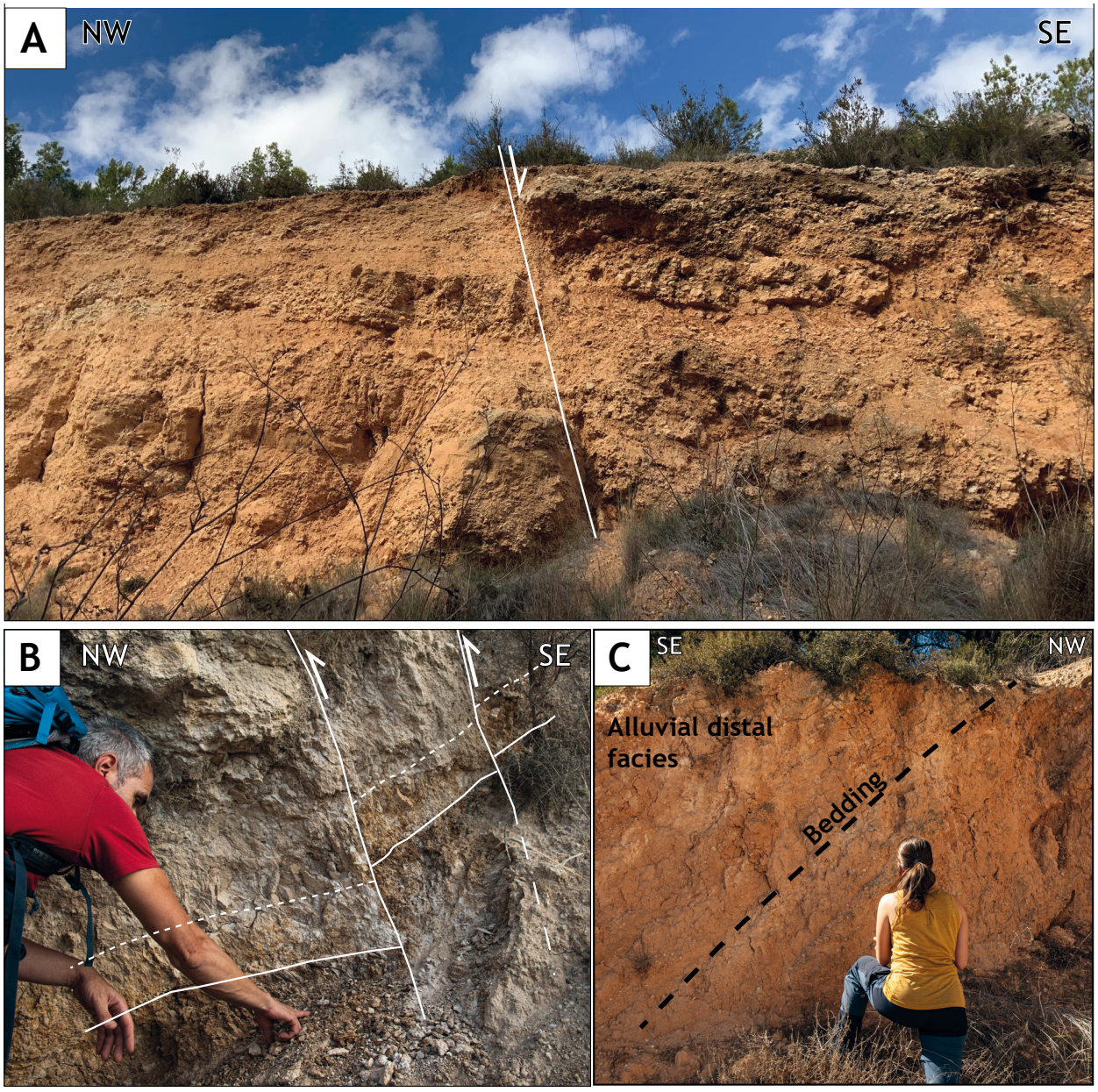

FIGURE 7. A) Pliocene alluvial materials offset by the intrabasinal fault. Picture location: 30S 721586.01 m E 4290059.55 m N; B) Messinian-Pliocene deposits deformed by a secondary fault of the intrabasinal fault zone, giving a local transpressive structure. Picture location: 30S 720255.89 m E 4288383.10 m N. C) North limb of the drag synform in Pliocene alluvial distal facies dipping more than 40º towards the basin. Picture location: 30S 720801.45 m E 4288517.67 m N. Projected coordinate system: ETRS 1989, UTM Zone 30N.

along the releasing bend could explain the presence of the thick alluvial fan deposits in this sector.

TECTONIC GEOMORPHOLOGY

The geomorphologic analysis of the AFZ aimed to identify evidence of recent tectonic activity. Three geomorphic indices have been calculated: the mountain front Smf (Bull and McFadden, 1977; Wells *et al.*, 1988), the Vf (Bull and McFadden, 1977), and the drainage Bs (Canon, 1976; Ramírez-Herrera, 1994). In addition, we carried out a qualitative analysis of the drainage network by mapping disturbed fluvial patterns (*e.g.* offset, beheaded, or captured valleys) and complemented by the visual analysis of 12 longitudinal river profiles crossing the fault.

Mountain front analysis

The mountain front generated by the AFZ was analysed from field and map observations and through the calculation

of the mountain front Smf. The mountain front has a length of 11.2 km with a mean N050E direction. The front can be divided into two portions corresponding to the two sectors of the AFZ (Fig. 8). In the SW sector, the mountain front is generated by the border fault strand. Therefore, this part of the mountain front consists of Oligocene limestones and cemented calcareous conglomerates. In the NE sector, the mountain front is generated by the intrabasinal strand. Therefore, in the NE sector, the mountain front developed in the continental Messinian to Pliocene lacustrine and alluvial succession.

Smf indices were calculated separately to evaluate the sinuosity of the mountain front in these two sectors. The value of the Smf index in the SW sector of the mountain front is of 1.10, while in the NE sector is of 1.16. The Smf index for the entire mountain front is 1.13. The differences between both sectors are almost insignificant, reflecting linear mountain fronts.

Drainage network analysis

The geomorphic analysis of the drainage network in the study area was performed by studying the drainage network geometry in relation to the fault (Fig. 9), the longitudinal profiles of the cross-fault streams (Fig. 10), and the calculation of the Vf (Table 2), and the drainage basin shape index (Table 2; Fig. 11) to these catchments.

The drainage network pattern reveals several left-lateral displacements and flow direction changes of the channels in the NE sector of the AFZ (Fig. 9). Some of these streams present segments that locally run subparallel or oblique to the intrabasinal fault trace at, or immediately up- or downstream of the fault traces (Fig. 9). These stream deflections can be interpreted as a consequence of the horizontal component of displacement of the AFZ.

The longitudinal profiles of 12 cross-fault streams (Fig. 10) reveal general morphologies ranging between convex-linear to slightly concave. In the SW sector, rivers present marked knickpoints in their profiles (*e.g.* streams [1], [2], and [4] in Fig. 10). These knickpoints coincide with the main fault escarpments, which generate steps in the topography. However, they are accentuated by the lithological contrast produced by the fault, which juxtaposes strongly cemented conglomerates and limestones in the northeastern block with soft erodible lacustrine marls and slightly cemented conglomerates in the southwestern block.

In the NE sector of the AFZ, the longitudinal stream profiles (Fig. 11: profiles [5] to [12]) present subtle gradient anomalies and steps. In this sector of the fault, the drainage

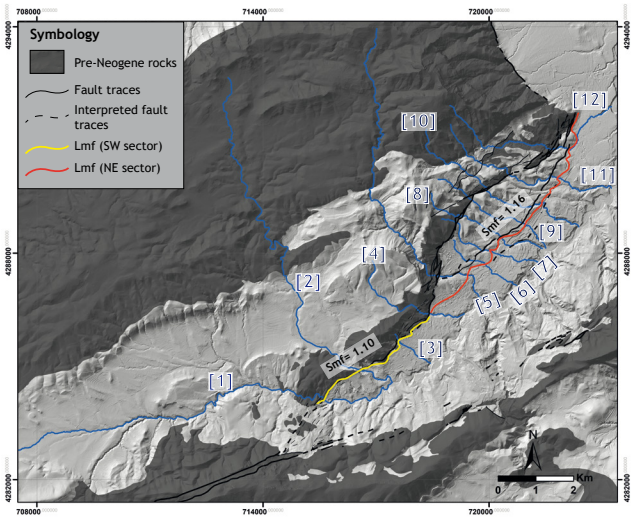

FIGURE 8. Hillshade map of the study area, extracted from the 2 m/pixel DEM, with the AFZ traces and the mountain front. Blue lines are the 12 streams selected for the drainage network analysis.

system is formed by gorges and valleys incised mainly into the Pliocene series and the Pleistocene alluvial deposits which are materials more erodible than the Oligocene cemented conglomerates and limestones. Consequently, the steeper segments of the profiles within the basin that are located at, or a small distance from the fault traces could be attributed to the tectonic activity of the AFZ. Lithology-related steps and high slope gradient anomalies are also visible in the headwater segments of these streams, far from any fault strand.

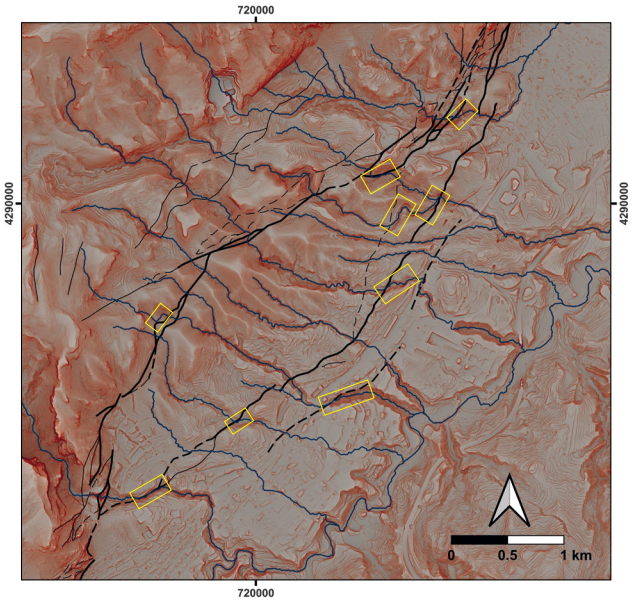

FIGURE 9. Red relief image map of the NE sector of the AFZ showing the fault traces and the main gorges/rivers. Yellow rectangles indicate fault-related left-lateral channel displacement.

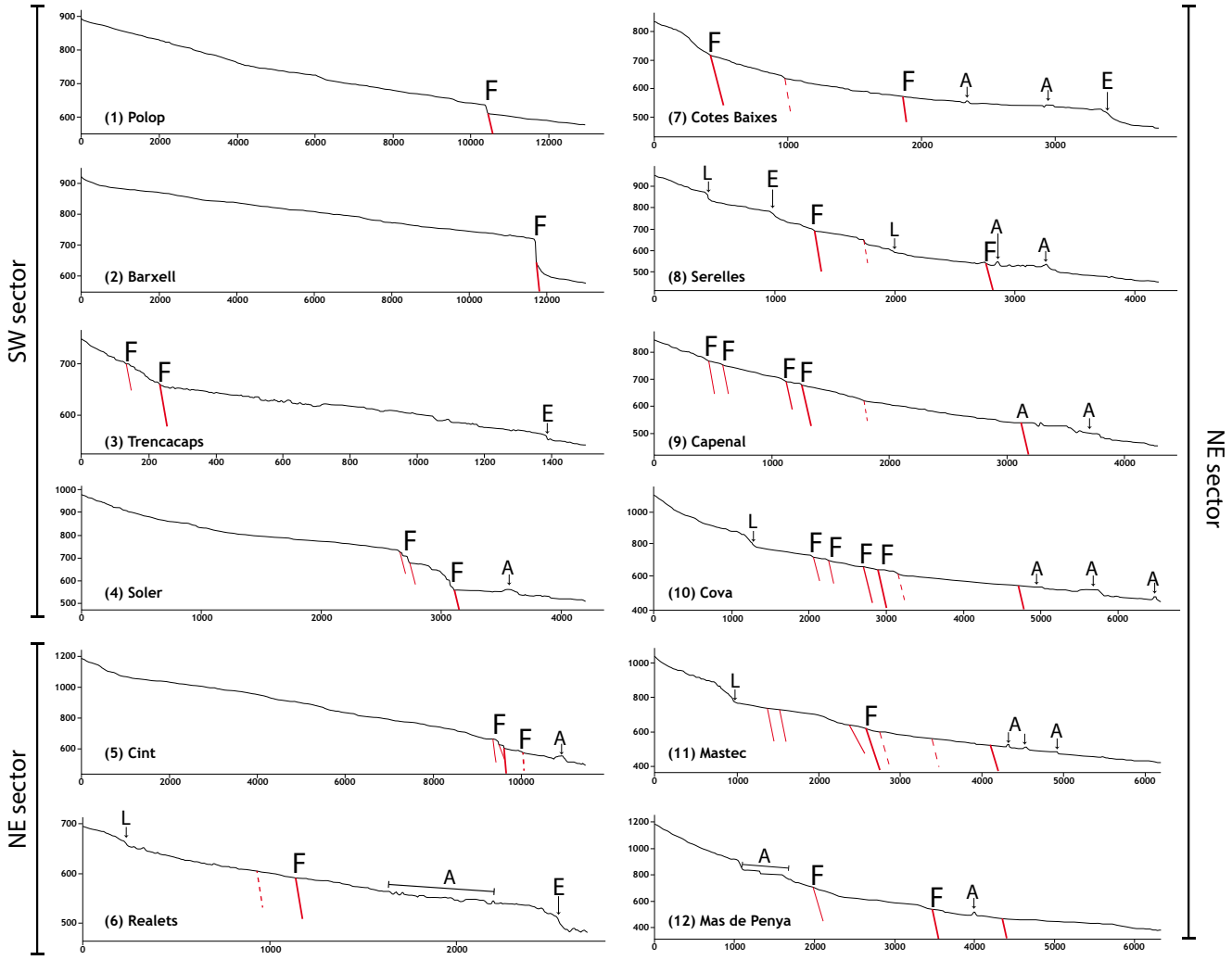

FIGURE 10. Longitudinal river profiles (location in Figure 8). Red lines mark the location of fault strands. Knickpoints: F= Fault-related; E= erosional (main river incision); L= Lithological contrasts; A= Anthropic landscape alterations such as artificial infills, bridges, and roads.

In some profiles, artificial infilling of stream channels and gullies generate flat surfaces that could be obscuring potential fault-related knickpoints. In addition, some peaks observed in the profiles are produced by roads or bridges crossing the streams, resulting in knickpoints of anthropic origin (*e.g.* in [9], [10], [11], and [12] profiles, Fig. 10).

Regarding the quantitative analysis of the drainage network, the obtained Vf values for the 12 selected streams range between 0.07 to 0.41, with a mean value of 0.28±0.11 (Table 2). These values indicate a V-shaped valley morphology. Moreover, there is no recognizable difference in the Vf ratio between streams of the SW sector (streams [1] to [4]) with a mean value of 0.23, and those of the NE sector (streams [5] to [12]) with a mean value of 0.26.

Additionally, the shape of the watersheds corresponding to the 12 selected stream was described and numerically analysed using the drainage Bs. In the SW sector, four watersheds developed crossing the fault zone. Watersheds in this sector present a larger area, especially the two southernmost ones (Fig. 11), which are the largest and show a well-developed drainage network. Bs values in the SW sector range from 1.50 to 2.1. On the contrary, in the NE sector, eight cross-fault watersheds developed (Fig. 11). These watersheds present common characteristics: they are regular and sub-parallel between them, have narrow, elongated shapes running sub-perpendicular to the mountain front and the fault scarps, and also show a poorly developed drainage system characterized by scarce to no tributary streams besides the main channel. The Bs in the NE sector displays higher values, ranging from 3.02 to 7.14 (Table 2; Fig. 11).

TABLE 2. Valley width/height ratio (Vf) and Basin shape index (Bs) values for each of the studied streams

Fault Sector	Numeration	Main Gorge/River	Vfw	Eld	Erd	Esc	Vf	Mean	Bl	Bw	Bs
SW	1	Polop	12.86	670.08	691.64	637.68	0.30	0.23	11050.82	6325.80	1.75
	2	Barxell	5.54	756.32	845.95	721.14	0.07		9817.15	5097.10	1.93
	3	Trencacaps	8.24	782.85	758.72	750.50	0.41		1583.51	734.76	2.16
	4	Soler	3.4	690.38	697.14	669.90	0.14		2885.89	1920.81	1.50
NE	5	Cint	5.64	625.88	608.41	564.11	0.11	0.26	7922.80	2625.92	3.02
	6	Realets	5.68	594.48	610.73	586.31	0.35		2216.44	310.28	7.14
	7	Cotes Baixes	11.16	612.04	595.93	573.41	0.37		3116.69	522.25	5.97
	8	Serelles	11.49	577.56	593.81	548.63	0.31		3776.29	634.39	5.95
	9	Capenal	4.95	557.27	571.41	542.80	0.23		3944.45	677.84	5.82
	10	Cova	11.05	568.02	572.38	538.83	0.35		5332.30	1685.94	3.16
	11	Mastec	6.07	570.02	546.11	535.50	0.27		4919.37	1233.11	3.99
	12	MasPenya	5.58	521.02	540.34	486.00	0.12		4432.68	1080.61	4.10
	Max Value						**0.41**				**7.14**
	Min Value						**0.07**				**1.50**
	Mean Value						**0.28**				**3.58**
	1σ						**0.11**				**1.94**

PALAEOSEISMOLOGICAL ANALYSIS

The most recent sediments in the study area primarily consist of fluvial terraces, as well as alluvial, and colluvial deposits. Until now, these deposits were previously assigned as Quaternary based on stratigraphic criteria due to the lack of fossil content (Almela *et al.*, 1973; Pierson d'Autrey, 1987). In this section, new radiocarbon dates and evidence of deformed Quaternary deposits are presented. We carried out a palaeoseismological analysis of the Cotes Altes site (see location in Fig. 3) where proximal colluvial-alluvial deposits are faulted (see detailed stratigraphic descriptions in Appendix I).

The Cotes Altes site is located to the north of Alcoy (UTM: 30S 718716.32 m E 4287698.31 m N; see location in Fig. 3). It consists of a vertical wall in a natural outcrop located on the fault bend near the end of the SW sector of the AFZ. In this area, the AFZ consists of N10E striking border fault planes (Fig. 3). These faults juxtapose Oligocene limestones with Quaternary colluvial deposits in the SE block. The fault zone in the studied site is up to 1.5 m thick, comprised by several fault strands (F0, F1, F2 and F3 in Fig. 12). A highly sheared band deforming both the Oligocene and the Quaternary deposits is observed. This shear band displays a fabric subparallel to the faults. This sheared band also includes F2 and F3 strands, both deforming the Quaternary deposits.

Surface rupture history

Cross-cutting relationships were used to identify potential palaeoearthquakes at Cotes Altes site. To date the interpreted palaeoearthquakes, we collected several samples for radiocarbon dating. The obtained dates were introduced in an OxCal model (See Appendix II; Bronk Ramsey, 2008, 2009).

Of all the collected samples, results from dating gastropod shells were not considered to build the earthquake chronology. This is because the sampled gastropods displayed ages younger than 3,000 years, so they must be excluded due to the phenomenon referred as the "Limestone Problem" (Goodfriend and Stipp, 1983). The phenomenon is caused by many taxa of large terrestrial gastropods when they incorporate inorganic carbon from carbonate rocks to

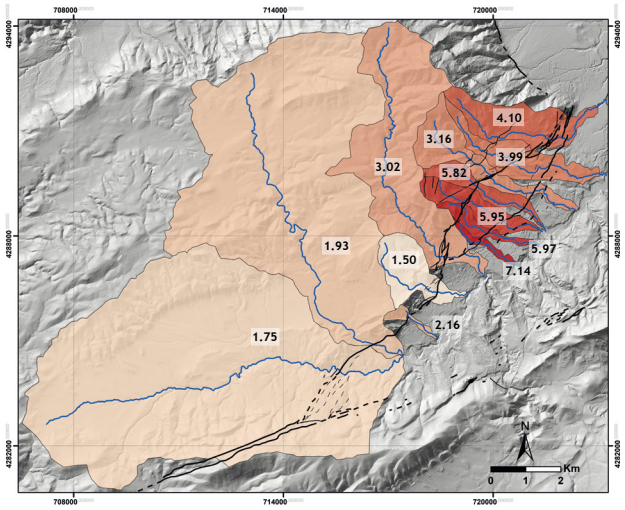

FIGURE 11. Map showing the streams used for the geomorphic analysis, the shape of their calculated watersheds and their Basin shape index (Bs) values.

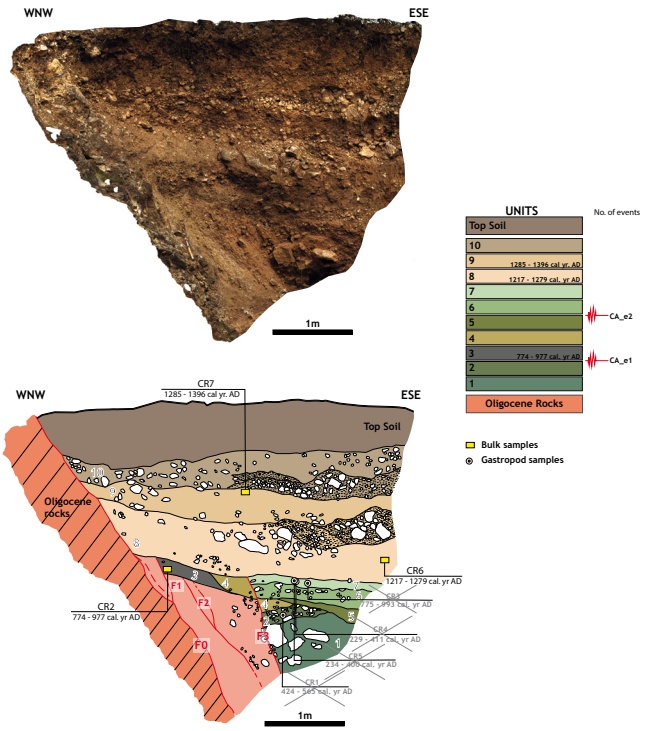

FIGURE 12. Log of the Cotes Altes site, depicting the described stratigraphic units, faults, and the collected samples The interpretation of the log, in terms of palaeoseismic stratigraphic units and number of events is also illustrated. Outcrop location: 30S 718719.67 m E 4287701.13 m N.

build their shells, what can cause the radiocarbon ages to be as much as ca. 3000 years older than they are.

The oldest event (CA_e1) is evidenced by the rupture of F2 strand, which is topped by Unit 3 (Fig. 12). This event lacks a lower constrain and is post-dated by the bulk radiocarbon sample CR2 in Unit 3. The OxCal model for CA_e1 yields an age range of 221- 982 AD (Fig. 13). The second event (CA_e2) is evidenced by a strand F1 offsetting Unit 3 and topped by Unit 8. Moreover, this event could be also responsible for the 20cm offset of Unit 4 by F3 (Fig. 12). The age of event CA_e2 is constrained by the bulk radiocarbon sample CR2 (lower constraint) and the bulk radiocarbon sample CR6 (upper constraint) (Fig. 12). The OxCal model thus yields an age range of 879–1258 AD for CA_e2 (Fig. 13).

DISCUSSION

The Alcoy Fault was firstly described by Pierson d'Autrey (1987) as a series of fault segments that were grouped into a single fault. This fault corresponds to the border strand of the AFZ, described in this work. This author stated that the activity of the border fault took place from the Early Miocene to the Messinian. García-Mayordomo (1998) extended the activity of this fault strand to the Pliocene based on the widespread backtilting of the Messinian-Pliocene series towards the fault, but no evidence of Pleistocene deformation was reported.

Zazo *et al.* (1993) and García-Mayordomo (1998) provided the preliminary surface trace of a second fault with a length of ca. 5 km, which in this work corresponds to the intrabasinal strand of the AFZ. Based on local pop-up structures within the fault zone, and on the geomorphological impact this fault strand had on some river channels, it was defined as a sinistral transpressive structure. These authors reported that the intrabasinal fault was an active structure during the Quaternary, based on the presence of displaced river channels incised in the Pleistocene alluvial deposits (inferred age later confirmed as Middle to Upper Pleistocene by Molina-Hernández *et al.*, 2015, 2016; Van Der Made and Montoya, 2007). García-Mayordomo (1998) further supported this statement with the seismicity in the area, that presents a pre-instrumental seismic record that evidences the occurrence of destructive events close to the AFZ, such as the 1547 Cocentaina earthquake (IEMS-98= VIII sensu Bisbal-

TABLE 3. Radiocarbon dates collected at the Cotes Altes site, in the Alcoy Fault Zone

Sample	Site	Type	Radiocarbon age		Calibrated age AD (95.4%)		Percentage of modern carbon (pMC)		D14C		Δ14C		IRMS δ13C
			BP	1σ error	From	To	pMC	1σ error	‰	1σ error	‰	1σ error	‰
CR7	CA1	Organic sediment	640	30	1285	1396	92.34	0.34	-76.58	3.44	-84.92	3.44	-24.05
CR6	CA1	Organic sediment	790	30	1217	1279	90.63	0.34	-93.66	3.38	-101.85	3.38	-23.96
CR5	CA1	Gastropod Shell	1760	30	234	400	80.32	0.3	-196.76	2.99	-204.01	2.99	-6.84
CR4	CA1	Gastropod Shell	2310	30	229	411	75.01	0.28	-249.91	2.8	-256.69	2.8	-7.82
CR3	CA1	Gastropod Shell	1130	30	775	993	86.88	0.32	-131.22	3.24	-139.07	3.24	-2.74
CR2	CA1	Organic sediment	1160	30	774	977	86.55	0.32	-134.46	3.23	-142.28	3.23	-23.89
CR1	CA1	Gastropod Shell	1570	30	424	565	82.25	0.31	-177.53	3.07	-184.96	3.07	-2.32

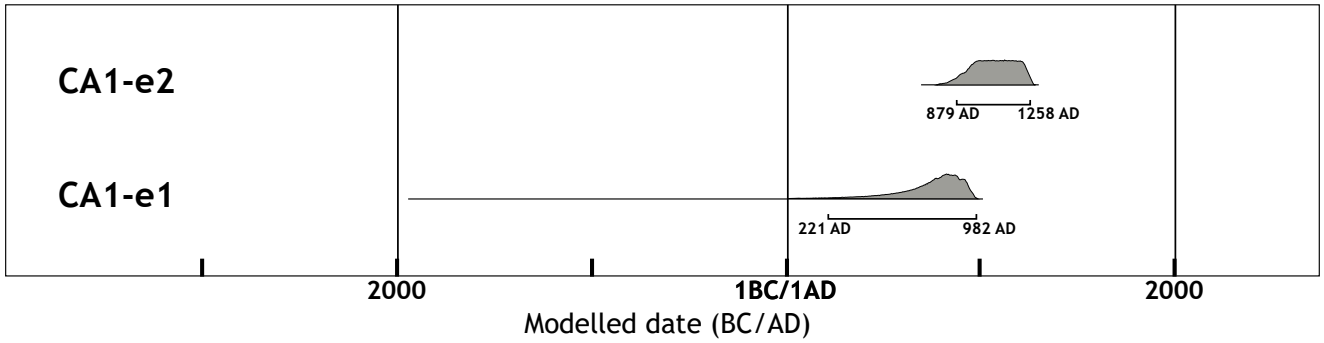

FIGURE 13. PDFs of the two identified palaeoearthquakes at the Cotes Altes site, obtained from the OxCal modelling.

Cervelló, 1984), or the 1620 Alcoy earthquake (IEMS-98= IX sensu Buforn and Udías, 2021, 2022; see epicenter location in Fig. 2). García-Mayordomo (1998) proposed the intrabasinal strand of the AFZ as the seismogenic source of both earthquakes. The AFZ is included in the Quaternary Active Fault Database of Iberia (Mayordomo *et al.*, 2012) as a "debated fault" since there is no consensus amongst the previous studies about which fault segments of the AFZ, if any, could produce surface ruptures in future earthquakes. This is mainly because of the absence of precise dating of the affected geomorphological features and because deformed Quaternary deposits had not been reported before.

The new structural and geomorphologic data presented in this study supports the left-lateral slip component proposed by Zazo *et al.* (1993), and García-Mayordomo (1998). This sense of slip applies for the entire AFZ, not only for the intrabasinal strand, as stated by these authors. This evidence include i) the measured oblique and sub-horizontal slickenlines, which indicate a strike-slip component, and ii) the displaced gullies and gorges along the fault trace reflecting a left-lateral sense of displacement.

Additionally, García-Mayordomo (1998) reported the intrabasinal strand as a transpressive structure, suggesting a reverse dip-slip component. The dip-slip component is supported by the majority of the measured oblique slickenlines. However, all the evidence points to a normal dip-slip component, meaning that the AFZ is a transtensive structure. First, the orientation of the slickenlines, plunging to the NE, along with the left-lateral main slip component, fits a secondary dip-slip where the southeastern block is the downthrown. Also, the development of the mountain front indicates an uplift of the northwestern block. Moreover, the widespread back-tilting of the Messinian-Pliocene rocks in the southeastern block, probably related to a listric geometry of the AFZ at depth, indicate that this secondary dip-slip component had a normal sense of displacement at least during all the Pliocene. However, the regional geodynamic setting has not changed since the Late Miocene, so the fault kinematics are likely the same during Quaternary times. These kinematics would be consistent with a WSW-ENE regional extension, but further geodesic assessments are necessary to confirm this regional geodynamic cadre.

Furthermore, it is worth considering whether the geometry and kinematics of the AFZ could be conditioned by the mobility of the Triassic evaporites located at the base of the Mesozoic succession of the Betic External Zones. The mechanical stratigraphy in the study area includes three main layers: an upper rigid layer consisting of Mesozoic-Quaternary sedimentary succession, a weak layer composed of Triassic salt, and an underlying rigid Variscan basement. This arrangement could lead to a decoupling between supra-salt faults, which slip may be conditioned by salt mobility, and deeper basement faults, driven by regional tectonics.

Since the formation of this Triassic layer, the Prebetic succession has been involved in several tectonic episodes that have produced salt mobilization. As a result, the salt layer is locally depleted, leading to the formation of salt wealds (*e.g.* Martin-Rojas *et al.*, in press; Ramos *et al.*, 2025) that may reduce the potential of the Triassic evaporites to act as a detachment level. On the other hand, seismic tomography studies realized to the north of the study area indicate that the main faults in the eastern Prebetic offset both the supra- and the sub-salt layers (Rubinat *et al.*, 2010, 2012). This structural connection between supra-salt and sub-salt structures is further supported by data obtained from seismic profiles in the SW Valencia Trough (Martin-Rojas *et al.*, in press). Based on these nearby examples, the AFZ could be considered as a fault that offsets both the supra-salt succession and the sub-salt basement. However, subsurface detailed studies in the Alcoy Basin should be necessary to shed light on this issue.

Quaternary activity of the Alcoy Fault Zone

Evidence of active tectonics influencing the development of the Quaternary landscape along the

AFZ is provided through the qualitative and quantitative geomorphic analysis. Some rivers crossing the NE sector of the AFZ developed a dog-legged geometry consisting of fault-subparallel channel segments that evolved in a left-lateral sense (Fig. 9). Since these streams are incised into Quaternary deposits (Middle to Upped Pleistocene alluvial deposits according to Van Der Made and Montoya (2007), Molina-Hernández *et al.* (2015, 2016)), the offset of gullies and gorges provides evidence for the Quaternary activity of the AFZ. Moreover, the longitudinal topographic profiles of rivers crossing both the SW and NE fault sectors show generally sub-linear to sub-convex shapes (Fig. 10). These morphologies are indicative of dynamic states that can be related to tectonic activity, lithological contrasts, and environmental or base level changes (Hack, 1973; Snyder *et al.*, 2000; Soria-Jáuregui *et al.*, 2018).

Despite the added complexity introduced by the high degree of anthropogenic modification in the area—which may have erased evidence of fault activity in the drainage network—several pronounced knickpoints can still be identified. Some of these knickpoints coincide with fault traces, producing steep topographic steps. In the case of the border strand, it is difficult to determine whether these knickpoints are solely the result of the fault activity, as they could also be the result of the lithological contrast. However, knickpoints that coincide with the intrabasinal fault trace can be interpreted as the result of fault displacement, since this fault juxtaposes analogous lithologies. Also, in this strand, knickpoints were also found a few meters upstream from the fault trace. This is the result of the high erodibility of the Messinian–Pliocene sediments, which causes an upwards migration of knickpoints due to headwards erosion (*e.g.* Bishop, 2007; Castillo *et al.*, 2014; Medina-Cascales *et al.*, 2021).

The results obtained through the application of the three morphometric indices suggests that the AFZ is tectonically active. The mountain front Smf present values of 1.10 for the SW sector and 1.16 for the NE sector, with a Smf value for the entire front of 1.13 (Fig. 8). These values categorize the mountain front of the AFZ as class 1, which correspond to active fronts according to Silva *et al.* (2003). The small difference in Smf values between both sectors seems to be primarily related to lithological differences. The SW front develops directly on the Oligocene rocks, composed of strongly cemented limestones and conglomerates, whereas the NE front coincides with the intrabasinal fault strand and is formed in the softer Messinian–Pliocene lacustrine–alluvial deposits, which are more susceptible to erosion. Remarkably, even in these softer materials, the mountain front maintains low sinuosity values. The obtained Smf values are similar to those calculated in other sectors with confirmed tectonic activity within the Betic Cordillera, such as the western segments of the active mountain front of Sierra Nevada (Pérez-Peña *et al.*, 2010), and those reported for the mountain front of the active Baza Fault (García-Tortosa *et al.*, 2008).

Additionally, the obtained Vf calculated for all the cross-fault catchments range from 0.07 to 0.41 (Table 2). These values indicate V-shaped valley morphologies associated with an active stream incision, which is characteristic of areas undergoing active uplift (Keller and Pinter, 2002; Bull, 2007, 2009). Furthermore, Vf values for the AFZ are independent on lithology. The obtained values for all the analysed valleys crossing the fault are low, whether they are incised into hard Oligocene rocks or softer basin infill deposits. This reinforces the interpretation that the pronounced entrenchment of these valleys is controlled by uplift associated with the AFZ and not by the erodibility of the underlying rocks.

Finally, Bs yielded values generally higher than 1.5 (Table 2). Bs values over 1 are indicative of elongated basins and are interpreted as tectonically active basins (Canon, 1976; Ramírez-Herrera, 1994). The tectonic control in watershed morphologies seems more accentuated in the NE fault sector. In this sector, watersheds are more elongated; with much higher Bs values (Table 2). Moreover, watersheds in the NE sector developed perpendicular to the mountain front, subparallel to each other in a regular pattern, and displaying very similar sizes and lengths. Additionally, they show a simple, immature drainage pattern (Fig. 9).

In addition, geological data evidencing fault activity during the Quaternary come from the analysed Cotes Altes palaeoseismological site. Data from this site indicate that the AFZ has produced at least two palaeoearthquakes during the past ~1,160 years (Fig. 13). As above discussed, these two events are dated as: 774–977 AD (CA_e1) and 879–1258 AD (CA_e2). Despite their recent ages, these events do not seem to correspond spatially and chronologically with any of the earthquakes within the historical records (see dates in Table 1). Hence, these events would represent an extension of the historical seismic catalogue.

The Holocene fault activity of the AFZ is further supported by the ongoing current seismic activity in the area. During the last years, the Alcoy Basin has been affected by low-magnitude earthquakes. However, there are some examples of higher magnitudes, such as the the 1941 (mbLg= 3.7) and the 2025 (mbLg= 3.2) events (IGN 2025). According to the locations of the epicenters (see Fig. 2) and the geometry of the AFZ, these earthquakes can be attributed to this fault. These earthquakes were not destructive but were perceived with relative intensity by the population in many towns in the vicinity of Alcoy city.

Finally, the presence of Triassic evaporites in the study area could raise the possibility that both the described surface

Quaternary deformation and the seismicity may reflect salt-related creep rather than tectonic displacement, implying that the AFZ is decoupled from basement faults. This has important implications for the seismic potential of the fault. If the AFZ is decoupled from basement faults, *i.e.* restricted to the supra-salt succession, the maximum seismogenic thickness of the fault would be lower, reducing its seismic potential. Conversely, if the AFZ offsets the entire succession and is mechanically linked to sub-salt basement structures, the thickness of the seismogenic crust involved during an event would be greater, resulting in higher seismic potential.

As discussed above, previous studies (Martin-Rojas *et al.*, in press; Rubinat *et al.*, 2010, 2012) lead us to consider the AFZ as a fault rooted in the Variscan basement, in the absence of subsurface data. In this case, the Quaternary evidence of activity of the AFZ is considered as result of regional tectonics. This assumption is also supported by historical seismicity, as such a significant event as the 1620 Alcoy earthquake should have been nucleated at a depth greater than the thickness of the supra-salt succession.

CONCLUSIONS

The Alcoy Fault Zone (AFZ) is a N045E, steeply dipping fault with a total length of 13 km. The structural characterization of the fault zone reveals oblique kinematics, with a main left-lateral component and a secondary vertical component, where the downthrown is the SE block of the fault. Two sectors are differentiated: i) A SW sector formed by a main border strand with an up to 800 m damage zone, and ii) a NE sector with an up to 2,100 m damage zone that consists of two main fault zones, a border strand and an intrabasinal strand.

Both fault zones present geomorphological and geological evidence of Quaternary activity. The geomorphic analysis reveals displaced river channels and gullies along the fault trace in a left-lateral sense. Moreover, all the geomorphic indices suggest an ongoing tectonic activity in the AFZ, resulting in a sublinear mountain front, highly incised gullies, and elongated, narrow, and subparallel watersheds.

Additionally, an analysis in an outcrop of deformed Holocene colluvial deposits yields the first palaeosismological results of the AFZ. These results indicate two rupturing events during the last ca. 1,160 years. These events allow to expand the historical seismic record, which is already characterized by the occurrence of several destructive earthquakes. Moreover, the AFZ would be the seeismogenic source of at least two significant instrumental earthqueakes, the 1941 (mbLg= 3.7) and the 2025 (mbLg= 3.2) events.

The new structural and palaeoseismological data on the Alcoy Fault Zone provide valuable insights for future seismogenic characterization of active structures and for seismic hazard assessments in the External Zones of the Betic Cordillera, a region where studies on active tectonics are very scarce. Our results also highlight the need for further investigations into other potentially active faults within the Alcoy Basin and across the northeastern sector of the eastern Betic Cordillera, with the aim of identifying seismogenic sources capable of generating destructive earthquakes.

ACKNOWLEDGMENTS

This work was funded by the research group VIGROB053 (University of Alicante), the research project AICO2021/196 of the Generalitat Valenciana (Valencia regional government). Eva Santamaría Pérez was funded by Ph.D. contract UAFPU21-94 of the University of Alicante. The Institut Cartogràfic Valencià also provided partial funding. We would also like to thank Menno de Ruig for all his suggestions and reviews.

REFERENCES

Alfaro, P., 1995. Neotectónica en la Cuenca del Bajo Segura (Extremo oriental de la Cordillera Bética). PhD Thesis. Alicante, Universidad de Alicante, 320pp.

Alfaro, P., Andreu, J.M., Delgado, J., Estévez, A., Soria, J.M., Teixidó, T., 2002. Quaternary deformation of the Bajo Segura blind fault (eastern Betic Cordillera, Spain) revealed by high-resolution reflection profiling. Geological Magazine, 139(3), 331-341.

Alfaro, P., Delgado, J., Sanz de Galdeano, C., Galindo- Zaldívar, J., García-Tortosa, F.J., López-Garrido, A.C., López-Casado, C., Marín-Lechado, A., Gil, A., Borque, M.J., 2008. The Baza Fault: a major active extensional fault in the central Betic Cordillera (south Spain). International Journal of Earth Sciences, 97, 1353-1365. DOI: https://doi.org/10.1007/s00531-007-0213-z

Alfaro, P., Andreu, J.M., Bartolomé, R., Borque, M.J., Estévez, A., García-Mayordomo, J., García-Tortosa, F.J., Gil, A.J., Gràcia, E., Lo Iacono, C., 2012. The Bajo Segura Fault Zone: Active blind thrusting in the Eastern Betic Cordillera (SE Spain). Journal of Iberian Geology, 38(1), 271-284. DOI: http://dx.doi.org/10.5209/rev_JIGE.2012.v38.n1.39217

Almela, A.S., Gómez, E.N., Quintero, I.A., Mansilla, H.I., 1973. Memoria asociada al mapa geolólogico de España 1: 50000, hoja nº 821. Madrid, Instituto Geológico y Minero de España (IGME), 33pp.

Argus, D.F, Gordon, R.G., DeMets, C., 2011. Geologically current motion of 56 plates relative to the no-net-rotation reference frame. Geochemistry, Geophysics, Geosystems, 12(11), Q11001. DOI: https://doi.org/10.1029/2011GC003751

Azéma, J., Foucault, A., Fourcade, E., García-Hernández, M., González-Donoso, J.M., Linares, A., Linares, D., López-Garrido, A.C., Rivas, P., Vera, J.A., 1979. Las microfacies del Jurásico y Cretácico de las Zonas Externas de las Cordilleras Béticas. Secretariado de Publicaciones. Universidad de Granada, 83pp.

Batlló, J., Martínez-Solares, J.M., Macià, R., Stich, D., Morales, J., Garrido, L., 2015. The autumn 1919 Torremendo (Jacarilla) earthquake series (SE Spain). Annals of Geophysics, 58(3), S0324. DOI: https://doi.org/10.4401/ag-6686

Bernabé-Maestre, J.M., 1975. Red fluvial y niveles de terrazas en la depresión Concentaina-Muro (Valls d'Alcoi). Cuadernos de geografía, 16, 23-39.

Bisbal-Cervelló, L., 1984. Estudio de las distribuciones de intensidades sísmicas en el ámbito Valenciano su incidencia en las obras públicas. Tomo V. Estudio monográfico de la serie sísmica del 23-3-1748 al 8-4-1748 con epicentro en Estubeny (tradicionalmente llamado "Terremoto de Montesa). PhD Thesis. Valencia, Universidad Politécnica de Valencia, 592pp.

Bishop, P., 2007. Long-term landscape evolution: linking tectonics and surface processes. Earth Surface Processes and Landforms, 32(3), 329-365. DOI: https://doi.org/10.1002/esp.1493

Borque, M.J., Sánchez-Alzola, A., Martin-Rojas, I., Alfaro, P., Molina, S., Rosa-Cintas, S., Rodríguez-Caderot, G., de Lacy, C., García-Armenteros, J.A., Avilés, M., Herrera-Olmo, A., García-Tortosa, F.J., Estévez, A., Gil, A.J., 2019. How much Nubia-Eurasia convergence is accommodated by the NE end of the Eastern Betic Shear Zone (SE Spain)? Constraints from GPS velocities. Tectonics, 38(5), 1824-1839. DOI: https://doi.org/10.1029/2018TC004970

Bousquet, J.C., 1979. Quaternary strike-slip faults in Southeastern Spain. Tectonophysics, 52(1-4), 277-286. DOI: https://doi.org/10.1016/0040-1951(79)90232-4

Bronk Ramsey, C., 2008. Deposition models for chronological records, Quaternary Science Reviews, 27(1-2), 42-60. DOI: https://doi.org/10.1016/j.quascirev.2007.01.019

Bronk Ramsey, C., 2009. Bayesian Analysis of Radiocarbon Dates. Radiocarbon, 51(1), 337-360. DOI: https://doi.org/10.1017/S0033822200033865

Buforn, E., Udías, A., 2021. El terremoto de Alcoy de 1620 y la serie sísmica de 1644 en la comarca. Centro Nacional de Información Geográfica, 140pp. DOI: https://doi.org/10.7419/162.07.2021

Buforn, E., Udías, A., 2022. The 1620 and 1644 Earthquakes in Alcoy and the Eastern Region of Spain. Seismological Research Letters 93(4), 2335-2346. DOI: https://doi.org/10.1785/0220220053

Buforn, E., Bezzeghoud, M., Udías, A., Pro, C., 2004. Seismic Sources on the Iberia-African Plate Boundary and their Tectonic Implications. Pure applied geophysics, 161, 623-646. DOI: https://doi.org/10.1007/s00024-003-2466-1

Bull, W.B., 2007. Tectonic Geomorphology of Mountains: A New Approach to Paleoseismology. Oxford (U.K.), Blackwell publishing, 320pp.

Bull, W.B., 2009. Geomorphic responses to climatic change. New Jersey, Blackburn Press, 326pp.

Bull, W.B., McFadden, L., 1977. Tectonic geomorphology north and south of the Garlock Fault, California. In: Doehring, D.O. (ed.). Geomorphology in Arid regions. Publications in Geomorphology, State University of New York at Bingamton, 115-139.

Canon, P.J., 1976. Generation of explicit parameters for a quantitative geomorphic study of the Mill Creek drainage basin. Oklahoma Geology Notes, 36(1), 3-16.

Canora, C., 2005. Evolución Neotéctónica de la Zona de Falla de Crevillente (Sector Occidental). Implicaciones Sismotectónicas. Tesina. Madrid, Universidad Complutense de Madrid, 132pp.

Canova, D.P., Cofrade, G., Roca, E., De Matteis, M., Ferrer, O., 2025. Where the salt sheet ends – submarine allochthonous salt advance and hindrance, The Elda Salt Sheet, Eastern Prebetics (Southern Iberia). Marine and Petroleum Geology, 182, 107598. DOI: https://doi.org/10.1016/j.marpetgeo.2025.107598

Carbonell, V., 1668. Celebre Centuria que consagró la ilustre y Real Villa de Alcoy a Honor y Culto del Soberano Sacramento del Altar. Valencia: por Iuan Lorenco Cabrera, 1672, 296pp.

Castillo, M., Muñoz-Salinas, E., Ferrari, L., 2014. Response of a landscape to tectonics using channel steepness indices (Ksn) and OSL: a case of study from the Jalisco Block, Western Mexico. Geomorphology, 221, 204-214. DOI: https://doi.org/10.1016/j.geomorph.2014.06.017

De Larouzière, F., Bolze, J.J., De Larouzière, F.D., Montenat, C., Ott d'Estevou, P., 1988. The Betic segment of the lithospheric trans-Alboran shear zone during the late Miocene. Tectonophysics, 152(1-2), 41-52. DOI: https://doi.org/10.1016/0040-1951(88)90028-5

Delgado, J., Giner, J., López-Casado, C., Auernheimer, C., 1993. Análisis de la respuesta del suelo en intensidades. Aplicación al terremoto de Torrevieja. In: Ortíz-Silla, R. (ed.). Problemática Geoambiental y Desarrollo, V Reunión Nacional de Geología Ambiental y Ordenación del Territorio. Murcia, Sociedad Española de Geología Ambiental y Ordenación del Territorio, II, 627-636.

Delgado, J., Peláez, J.A., Tomás, R., Estévez, A., López Casado, C., Doménech, C., Cuenca, A., 2006. Evaluación de la susceptibilidad de las laderas a sufrir inestabilidades inducidas por terremotos: aplicación a la cuenca de drenaje del río Serpis (provincia de Alicante). Revista de la Sociedad Geológica de España, 19(3-4), 197-218.

Delgado, J., Peláez, J.A., Tomás, R., García-Tortosa, F.J., Alfaro, P., López-Casado, C., 2011. Seismically-induced landslides in the Betic Cordillera (S Spain). Soil Dynamics and Earthquake Engineering, 31(9), 1203-1211. DOI: https://doi.org/10.1016/j.soildyn.2011.04.008

DeMets, C., Gordon, R.G., Argus, D.F., 2010. Geologically current plate motions. Geophysical Journal International, 181(1), 1-80. DOI: https://doi.org/10.1111/j.1365-246X.2009.04491.x

Echeverria, A., Khazaradze, G., Asensio, E., Gárate, J., Martín-Dávila, J., Suriñach, E., 2013. Crustal deformation in eastern Betics from CuaTeNeo GPS network. Tectonophysics, 608, 600-612. DOI: https://doi.org/10.1016/j.tecto.2013.08.020

Echeverria, A., Khazaradze, G., Asensio, E., Masana, E., 2015. Geodetic evidence for continuing tectonic activity of the Carboneras Fault (SE Spain). Tectonophysics, 663, 302-309. DOI: https://doi.org/10.1016/j.tecto.2015.08.009

Estrella, M.J., Fumanal, M.P., Garay, P., 1993. Evolución geomorfológico de los valles Prebéticos Nororientales. Cuaternario y Geomorfología, 7, 157-170.

Fallot, P., 1948. Les Cordillères Bétiques. Estudios Geológicos, 4, 83-172.

Fumanal, M.P., 1994. El yacimiento musteriense de El Salt (Alcoi, País Valenciano): rasgos geomorfológicos y climatoestratigrafía de sus registros. SAGVNTVM. Papeles del Laboratorio de Arqueología de Valencia, 27, 39-55.

Galindo-Zaldívar, J., Borque, M.J., Pedrera, A., Marín-Lechado, C., Gil, A.J., López-Garrido, A.C., 2013. Deformation behaviour of the low-rate active Balanegra Fault Zone from high-precision levelling (Betic Cordillera, SE Spain). Journal of Geodynamics, 71, 43-51. DOI: https://doi.org/10.1016/j.jog.2013.07.003

García-Hernández, M., López-Garrido, A.C., Rivas, P., Sanz de Galdeano, C., Vera, J.A., 1980. Mesozoic paleogeographic evolution of the External Zones of the betic Cordillera. Geologie en Mijnbouw, 59(2), 155-168.

García-Mayordomo, J., 1998. Riesgo Sísmico en la Cuenca de Alcoy (Alicante). Aproximación a una Zonificación Sísmica. Tesina de Máster. Madrid, Universidad Complutense de Madrid, 100pp.

García-Mayordomo, J., 2005. Caracterización y Análisis de la Peligrosidad Sísmica en el Sureste de España. PhD Thesis. Madrid, Universidad Complutense de Madrid, 373pp.

García-Mayordomo, J., Martínez-Díaz, J.J., Arcos, A., Blázquez, R., 2002. Estudio Preliminar de la Paleosismicidad de la Falla de Benasau (Cuenca de Alcoy, Alicante). Valencia 4-8 de Febrero de 2002, 3ª Asamblea de Geodesia y Geofísica, Memorias, Tomo I, 412-415.

García-Mayordomo, J., Insua-Arévalo, J.M., Martínez-Díaz, J.J., Jiménez-Díaz, A., Martín-Banda, R., Martín-Alfageme, S., Álvarez-Gómez, J.A., Rodríguez-Peces, M., Pérez-López, R., Rodríguez-Pascua, M.A., Masana, E., Perea, H., Martín-González, F., Giner-Robles, J., Nemser, E.S., Cabral, J., the QAFI Compilers Working Group, 2012. The Quaternary Faults Database of Iberia (QAFI v.2.0). Journal of Iberian Geology, 38(1), 285-302. DOI: https://doi.org/10.5209/rev_JIGE.2012.v38.n1.39219

García-Molero, A., 1621. Relación muy verdadera de un caso muy espantoso y lastimoso en la villa de Alcoy Reyno de Valencia sucedió, Miercoles dos de Diziembre deste año passado de 1620, Granada: Pedro de Belmas y Francisco Heylan, 4pp.

García-Tortosa, F.J., Alfaro, P., Galindo-Zaldívar, J., Gibert, L., López-Garrido, A.C., Sanz de Galdeano, C., Ureña, M., 2008. Geomorphologic evidence of the active Baza fault (Betic Cordillera, South Spain). Geomorphology, 97(3-4), 374-391. DOI: https://doi.org/10.1016/j.geomorph.2007.08.007

Giner, J.J., Molina, S., Jáuregui, P.J., 2003. Sismicidad en la Comunidad Valenciana. Física de la Tierra, 15, 163-187.

Goodfriend, G.A., Stipp, J.J., 1983. Limestone and the problem of radiocarbon dating of land-snail shell carbonate. Geology, 11(10), 575-577. DOI: https://doi.org/10.1130/0091-7613(1983)11<575:LATPOR>2.0.CO;2

Goy, J.L., Rey, J., Díaz del Río, V., Zazo, C., 1987. Relación entre las unidades morfológicas cuaternarias del litoral y de la Plataforma intermedia-media de Valencia (España): implicaciones paleogeográficas. In: 3ª Reunión de Geología Ambiental y Ordenación del Territorio. Valencia, febrero de 1987, Universitat de Valencia, 2, 1351-1369.

Hack, J.T., 1973. Stream-profiles analysis and stream-gradient index. Journal of Research of the U.S. Geological Survey, 1(4), 421-429.

Instituto Geográfico Nacional (IGN). Catálogo de terremotos. Last accessed: February 2026. Website: https://www.ign.es/web/sis-catalogo-terremotos. DOI: https://doi.org/10.7419/162.03.2022

Keller, E.A., Pinter, N., 2002. Active Tectonics: Earthquakes, Uplift and Landscape. In: Lynch, P., Dellas, K. (eds.). Upper Saddle River. New Jersey (USA), Prentice-Hall, 362pp.

López-Casado, C., Estévez, A., Pina, J.A., Sanz de Galdeano, C., 1987. Alineaciones sismotectónicas en el sudeste de España. Ensayo de delimitación de fuentes sísmicas. Mediterranea, Serie de Estudios Geológicos, 6, 5-38.

López-Marinas, J.M., 1981. ¿Uno o dos terremotos catastróficos a fines del siglo XIV en el Reino de Valencia? Revista del Instituto de Estudios Alicantinos, 36, 59-72.

Madarieta-Txurruka, A., Galindo-Zaldívar, J., González-Castillo, L., Peláez, J.A., Ruiz-Armenteros, A.M., Henares, J., Garrido-Carretero, M.S., Avilés, M., Gil, A.J., 2021. High- and low-angle normal fault activity in a collisional orogen: The northeastern Granada Basin (Betic Cordillera). Tectonics, 40(7), e2021TC006715. DOI: https://doi.org/10.1029/2021TC006715

Mansino, S., Fierro, I., Ruiz-Sánchez, F.J., Montoya, P., 2013. The fossil rodent faunas of the localities Alcoy 2C and 2D (Alcoy Basin, Spain). Implications for dating the classical locality of Alcoy-Mina. Journal of Iberian Geology, 39(2), 261-284. DOI: http://dx.doi.org/10.5209/rev_JIGE.2013.v39.n2.42501

Marín-Lechado, C., Galindo-Zaldívar, J., Rodríguez-Fernández, L.R., Serrano, I., Pedrera, A., 2005. Active faults, seismicity and stresses in an internal boundary of a tectonic arc (Campo de Dalías and Níjar, southeastern Betic Cordilleras, Spain). Tectonophysics, 396(1-2), 81-96. DOI: https://doi.org/10.1016/j.tecto.2004.11.001

Marín-Lechado, C., Galindo-Zaldívar, J., Gil, A.J., Borque, M.J., de Lacy, M.C., Pedrera, A., López-Garrido, A.C., Alfaro, P., García-Tortosa, F., Ramos, M.I., Rodríguez-Caderot, G., Rodríguez-Fernández, J., Ruiz-Constán, A., Sanz de Galdeano, C., 2010. Levelling profiles and a GPS network to monitor the active folding and faulting deformation in the Campo de

Dalias (Betic Cordillera, Southeastern Spain). Sensors, 10(4), 3504-3518. DOI: https://doi.org/10.3390/s100403504

Martin-Rojas, I., Alfaro, P., Estévez, A., 2014. Tectonic evolution of the Bajo Segura Basin northern limit. Implications for the Crevillente Fault Evolution. Cuaternario y Geomorfología, 28(3-4), 85-94.

Martin-Rojas, I., Alfaro, P., Estévez, A., 2015. 3D geometry of growth strata in a fault-propagation fold. Insights into space-time evolution of the Crevillente Fault (Abanilla-Alicante sector), Betic Cordillera, Spain. International Journal of Earth Sciences, 104, 1387-1404. DOI: https://doi.org/10.1007/s00531-015-1143-9

Martin-Rojas, I., Ramos, A., de Ruig, M.J., Medina-Cascales, I., Santamaría-Pérez, E., Alfaro, P., in press. Influence of salt-related mechanical layering on the seismic potential of active faults: insights from the southwestern Valencia Trough (W Mediterranean). Natural Hazards and Earth Systems Sciences.

Martínez del Olmo, W., Leret Verdú, G., Suárez-Alba, J., 1986. La estructuración diapírica del Sector Prebético. Geogaceta, 1, 43-44.

Martínez-Solares, J.M., Mezcua, J., 2002. Catálogo sísmico de la Península Ibérica (880 AC-1900). Madrid (Spain), Monografía nº 18 Instituto Geográfico Nacional, 254pp.

Martino, S., Battaglia, S., Delgado, J., Esposito, C., Martini, G., Missori, C., 2018. Probabilistic approach to provide scenarios of earthquake-induced slope failures (PARSIFAL) applied to the Alcoy Basin (South Spain). Geosciences, 8(2), 57. DOI: https://doi.org/10.3390/geosciences8020057

Medina-Cascales, I., Garcia-Tortosa, F.J., Martin-Rojas, I., Perez-Pena, J.V., Alfaro, P., 2021. Tectonic geomorphology of an active slow-moving, intrabasinal fault: The Galera Fault (Guadix-Baza Basin, central Betic Cordillera, southern Spain). Geomorphology, 393, 107941. DOI: https://doi.org/10.1016/j.geomorph.2021.107941

Molina-Hernández, F.J., Vinagre, A.T., Santos, B.G., Gómez, C.M.H., 2015. Estudio geoarqueológico de áreas de aprovisionamiento de sílex en el Prebético de Alicante: Los ejemplos de Penella (Alcoi) y La Fenasosa (Onil). In: Alapont, L., Martí, J., Tendero, F. (eds.). Actuacions sobre el Patrimoni Arqueològic de la Comunitat Valenciana: actes de les I Jornades d'Arqueologia de la Comunitat Valenciana. Valencia, Ayuntamiento de Valencia, 13-27.

Molina-Hernández, F.J., Tarriño-Vinagre, A., Galván-Santos, B., Hernández-Gómez, C.M., 2016. The Flint of the Prebetic of Alicante: Types, variability and Pleistocene catchment and kapping areas. Cuadernos de Prehistoria y Arqueología de la Universidad de Granada, 26, 283-311.

Montenat, C., Ott d'Estevou, P., Masse, P., 1987. Tectonic-sedimentary characters of the Betic Neogene basins evolving in a crustal transcurrent shear zone (SE Spain). Elf-Aquitaine, Bulletin des Centres de Recherches Exploration Production, 11(1), 1-22.

Moseley, F., Cuttell, J.C., Lange, E.W., Stevens, D., Warbrick, J.R., 1981. Alpine tectonics and diapiric structures in the Pre-Betic zone of southeast Spain. Journal of Structural Geology, 3(3), 237-251. DOI: https://doi.org/10.1016/0191-8141(81)90020-1

Nocquet, J.M., 2012. Present-day kinematics of the Mediterranean: A comprehensive overview of GPS results. Tectonophysics, 579, 220-242. DOI: https://doi.org/10.1016/j.tecto.2012.03.037

Ordóñez-Delgado, S., Cuevas-González, J., Benavente, D., García del Cura, M., 2016. Architecture of Pleistocene fluvial tufa systems associated with waterfalls: El Salt (Alcoy, Spain). Geogaceta, 59, 7-10.

Ott D'Estevou, P., Montenat, C., Ladure, F., Pierson d'Autrey, L., 1988. Evolution tectono-sedimentaire du domaine Prébétique oriental (Espagne) au Miocene. Comptes Rendus de l'Académie des Sciences, 307(2), 789-796.

Pedrera, A., Marín-Lechado, C., Galindo-Zaldívzar, J., García-Lobón, J.L., 2014. Control of preexisting faults and near-surface diapirs on geometry and kinematics of fold-and-thrust belts (Internal Prebetic, Eastern Betic Cordillera). Journal of Geodynamics, 77, 135-148. DOI: https://doi.org/10.1016/j.jog.2013.09.007

Perea, H., Gràcia, E., Alfaro, P., Bartolomé, R., Lo Iacono, C., Moreno, X., Masana, E., EVENT SHELF Team, 2012. Quaternary active tectonic structures in the offshore Bajo Segura basin (SE Iberian Peninsula – Mediterranea Sea). Natural Hazards and Earth System Sciences, 12(10), 3151-3168. DOI: https://doi.org/10.5194/nhess-12-3151-2012

Pérez-Peña, A., Azor, A., Azañón, J.M., Keller, E.A., 2010. Active tectonics in the Sierra Nevada (Betic Cordillera, SE Spain): Insights from geomorphic indexes and drainage pattern analysis. Geomorphology, 119(1-2), 74-84. DOI: https://doi.org/10.1016/j.geomorph.2010.02.020

Pierson d'Autrey, L., 1987. Sédimentation et structuration synsédimentaire dans le bassin néogène d'Alcoy (Cordillères bétiques externes orientales, Espagne). PhD Thesis. Paris, Université de Paris-Sud (Centre d'Orsay), 314pp.

Ramírez-Herrera, M.T., 1994. Tectonic Geomorphology of the Acambay graben, Central Mexican Volcanic Belt. PhD Thesis. Edinburgh, University of Edinburgh, 288pp.

Ramos, A., De Ruig, M., Pedrera, A., Alfaro, P., Martin-Rojas, I., 2025. Salt expulsion triggered by prograding clinoforms in the SW Valencia Trough (SE Spain). Marine and Petroleum Geology, 173, 107268. DOI: 10.1016/j.marpetgeo.2024.107268

Roca, E., Sans, M., Koyi, H., 2006. Polyphase deformation of diapiric areas in models and in the eastern Prebetics (Spain). American Association of Petroleum Geologists Bulletin, 90(1), 115-136. DOI: https://doi.org/10.1306/07260504096

Rodríguez-Pascua, M.A., Pérez-López, R., Calvo, J.P., García del Cura, M.A., 2008. Recent seismogenic fault activity in a Late-Quaternary closed-lake graben basin (Albacete, Spain). Geomorphology, 102(1), 169-178.

Rodríguez-Pascua, M.A., Pérez-López, R., Garduño-Monroy, V.H., Giner-Robles, J.L., Silva, P.G., Perucha-Atienza, M.A., Hernández-Madrigal, V.M., Bischoff, J.L., 2012. Paleosesimic and geomorphologic evidence of recent tectonic activity of

the Pozohondo Fault (Betic Cordillera, SE Spain). Journal of Iberian Geology, 38(1), 239-251. DOI: https://doi.org/10.5209/rev_JIGE.2012.v38.n1.39216

Ruano, P., Galindo-Zaldívar, J., Jabaloy, A., 2004. Recent Tectonic Structures in a Transect of the Central Betic Cordillera. Pure and applied geophysics, 161, 541-563. DOI: https://doi.org/10.1007/s00024-003-2462-5

Rubinat, M., Ledo, J., Roca, E., Rosell, O., Queralt, P., 2010. Magnetotelluric characterization of a salt diapir: a case study on Bicorb-Quesa Diapir (Prebetic Zone, SE Spain). London, Journal of the Geological Society, 167, 145-153. DOI: 10.1144/0016-76492009-029

Rubinat, M., Roca, E., Escalas, M., Queralt, P., Ferrer, O., Ledo, J.J., 2012. The influence of basement structure on the evolution of the Bicorb-Quesa Diapir (eastern Betics, Iberian Peninsula): contractive thin-skinned deformation above a pre-existing extensional basement fault. International Journal of Earth Sciences, 102(2013), 25-41. DOI: 10.1007/s00531-012-0789-9

Rueda, J., Mezcúa, J., Sanchez-Ramos, M., 1996. La serie sísmica de Adra (Almería) de 1993 – 1994 y sus principales consecuencias sismotectónicas. Madrid, Avances en Geofísica y Geodesia, Instituto Geográfico Nacional, 91-98.

Sánchez-Alzola, A., Borque, M.J., Martín-Rojas, I., García-Tortosa, F., Alfaro, P., Estévez, A., Molina, S., Rodríguez-Calderot, G., de Lacy, C., García-Armenteros, J.A., Avilés, M., Herrera-Olmo, A., Rosa, G., Gil, A.J., 2014. Tasas de deformación GPS, en la cuenca del Bajo Segura (Cordillera Bética Oriental). Geogaceta, 56, 3-6.

Sanz de Galdeano, C.S., Shanov, S., Galindo-Zaldívar, J., Radulov, A., Nikolov, G., 2010. A new tectonic discontinuity in the Betic Cordillera deduced from active tectonics and seismicity in the Tabernas Basin. Journal of Geodynamics, 50(2), 57-66. DOI: https://doi.org/10.1016/j.jog.2010.02.005

Sanz de Galdeano, C., García-Tortosa, F.J., Peláez; J.A., Alfaro, P., Azañón, J.M., Galindo-Zaldívar, J., López Casado, C., López Garrido, A.C., Rodríguez-Fernández, J., Ruano, P., 2012. Main active faults in the Granada and Guadix-Baza Basins (Betic Cordillera). Journal of Iberian Geology. 38(1), 209-223. DOI: https://doi.org/10.5209/rev_JIGE.2012.v38.n1.39215

Schumm, S.A., Dumont, J.F., Holbrook, J.M., 2000. Active Tectonics and Alluvial Rivers. Cambridge, Cambridge University Press, 276pp.

Serpelloni, E., Vannucci, G., Pondrelli, S., Argnani, A., Casula, G., Anzidei, M., Balde, P., Gasperini, P., 2007. Kinematics of the Western Africa-Eurasia plate boundary from focal mechanisms and GPS data. Geophysical Journal International, 169(3), 1180-1200. DOI: https://doi.org/10.1111/j.1365-246X.2007.03367.x

Silva, P.G., Goy, J.L., Somoza, L., Zazo, C., Bardaji, T., 1993. Landscape response to strike-slip faulting linked to collisional settings: Quaternary tectonics and basin formation in the Eastern Betics, southeastern Spain. Tectonophysics, 224(4), 289-303. DOI: https://doi.org/10.1016/0040-1951(93)90034-H

Silva, P., Goy, J., Zazo, C., Bardaji, T., 2003. Fault-generated mountain fronts in southeast Spain: geomorphic assesstment of tectonic and seismic activity. Geomorphology, 50(1-3), 203-225. DOI: https://doi.org/10.1016/S0169-555X(02)00215-5

Snyder, N.P., Whipple, K.X., Tucker, G.E., Merritts, D.J., 2000. Landscape response to tectonic forcing: digital elevation model analysis of stream profiles in the Mendocino triple junction region, northern California. Geological Society of America Bulletin, 112(8), 1250-1263.

Soria, J.A., Alfaro, P., Fernández, J., Viseras, C., 2001. Quantitative subsidence-uplift analysis of the Bajo Segura Basin (eastern Betic Cordillera): tectonic control on the stratigraphic architecture. Sedimentary Geology, 140(3-4), 271-289. DOI: https://doi.org/10.1016/S0037-0738(00)00189-5

Soria-Jáuregui, A., Jiménez-Cantizano, F., Antón, L., 2018. Geomorphic and tectonic implications of the endorheic to exorheic transition of the Ebro River system in Northeast iberia. Quaternary Research, 91(2), 472-492. DOI: https://doi.org/10.1017/qua.2018.87

Taboada, A., Bousquet, J.C., Philip, H., 1993. Coseismic elastic models of folds above blind thrusts in the Betic Cordilleras (Spain) and evaluation of seismic hazard. Tectonophysics 220(1-4), 223-241. DOI: https://doi.org/10.1016/0040-1951(93)90233-A

Tomás, R., Díaz, E., Szeibert, W.T., Liu, X., Lopez-Sanchez, J.M., Zhao, C., 2023. Geomorphological characterization, remote sensing monitoring, and modeling of a slow-moving landslide in Alcoy (Southern Spain). Landslides, 20, 1293-1301. DOI: https://doi.org/10.1007/s10346-023-02032-8

Van Balen, R.T., Forzoni, A., Van Dam, J.A., 2015. Active faulting and folding along the Jumilla Fault Zone, northeastern Betics, Spain. Geomorphology, 237, 88-97. DOI: https://doi.org/10.1016/j.geomorph.2013.12.001

Van der Made, J., Montoya, P., 2007. Rinocerontes del Pleistoceno de El Baradello, Plaça de la República y El Molinar en Alcoy, España. Recerques del Museu d'Alcoi, 16, 7-18.

Wells, S.G., Bullard, T.F., Menges, C.M., Drake, P.G., Karas, P.A., Kelson, K.I., Ritter, J.B., Wesling, J.R., 1988. Regional variations in tectonic geomorphology along a segmented convergent plate boundary, Pacific coast of Costa Rica. Geomorphology, 1(3), 239-265. DOI: https://doi.org/10.1016/0169-555X(88)90016-5

Zazo, C., Goy, J.L., Silva, P., 1993. Actividad neotectónica cuaternaria en la cuenca neógena de Alcoy (España). Aplicación de criterios geomorfológicos. In: Ministerio de Ciencia y Tecnología, Instituto Tecnológico Geominero de España (eds.). El Cuaternario en España y Portugal. Madrid, Instituto Tecnológico Geominero de España (ITGE), 2, 691-696.

Manuscript received July 2025;
revision accepted January 2025;
published February 2026.

APPENDIX I. DETAILED STRATIGRAPHY OF THE COTES ALTES SITE

The Quaternary colluvial deposits can be subdivided in ten stratigraphic units (see Fig. 12). Unit 1 is a monomictic matrix-supported breccia with decimetric angular boulders. Matrix consists of grey, silty microconglomerates. Unit 2 is a matrix-supported breccia made up of poorly sorted centimetric clasts. The matrix is a silty dark-grey microconglomerate with some scarce gasteropod shells. Unit 4 is formed by millimetric to centimetric gravels with a silty grey matrix and some carbonate clasts. Unit 5 is a wedge-shaped body that thins to the north, comprising brown matrix-supported microconglomerates. Unit 6 consists of grain-supported gravels comprising poorly sorted millimetric to centimetric clasts. Unit 7 is a level formed by cemented coarse sand to micronconglomerates with silty brownish grey matrix. This unit is also characterized by the presence of gastropod shells.

Between F0 and F3 there is a ca. 1 m thick band of sheared red and greenish silts belonging to the colluvial deposits. This band is interpreted as the result of the shearing of Units 1 and 2. Unconformably overlying these silts there is a black level (Unit 3) comprising sandy silts with thin microconglomeratic layers and some sub-angular carbonate clasts. Moreover, Unit 3 is partially eroded to the east by a unit formed by millimetric to centimetric gravels with a silty grey matrix that is interpreted as Unit 4.

Unit 8 overlies all these units and consists of brown sandy silts with centimetric to decimetric angular carbonate boulders. This unit has some darker pure silt levels. Over Unit 8 lies Unit 9, which is formed by dark sandy silts with carbonate centimetric clasts and some channel-shaped bodies of oligomictic centimetric to decimetric gravels without matrix. This unit was also sampled for bulk radiocarbon dating. On top of this deposit is Unit 10, consisting of grain-supported gravels with channel-like bodies. Over Unit 10 a topsoil layer is developed with an erosive base and abundant plant roots. It consists of loose dark sandy clays with some carbonate pebbles.

APPENDIX II. OXCAL MODEL SCRIPT

```
Plot()
{
Sequence("COTES_ALTES1")
{
Boundary("Base");
Phase("Basament")
{
};
Zero_Boundary("Base_model");
Boundary("EQ1");
Phase("Black")
{
R_Date("CR2", 1160, 30);
};
Phase("u3")
{
};
Date("EQ2");
Phase("u7")
{
R_Date("CR6", 790, 30);
};
Phase("u8")
{
R_Date("CR7", 640, 30);
};
Phase("u9")
{
};
Phase("top_soil")
{
};
Boundary("Top");
};
```